PLOS NEGLECTED TROPICAL DISEASES

RESEARCH ARTICLE

Identification of a critical role for ZIKV capsid α3 in virus assembly and its genetic interaction with M protein

Anastazia Jablunovsky[1], **Anoop Narayanan**[1], **Joyce Jose**[1,2]*

1 Department of Biochemistry and Molecular Biology, The Pennsylvania State University, University Park, Pennsylvania, United States of America, **2** The Huck Institutes of the Life Sciences, The Pennsylvania State University, University Park, Pennsylvania, United States of America

* jxj321@psu.edu

Citation: Jablunovsky A, Narayanan A, Jose J (2024) Identification of a critical role for ZIKV capsid α3 in virus assembly and its genetic interaction with M protein. PLoS Negl Trop Dis 18(1): e0011873. https://doi.org/10.1371/journal.pntd.0011873

Editor: Michael W. Gaunt, Solena Ag, UNITED STATES MINOR OUTLYING ISLANDS

Received: August 7, 2023

Accepted: December 19, 2023

Published: January 2, 2024

Data Availability Statement: All data are presented in the manuscript and supporting information files.

Funding: This work was supported by Penn State University start-up funds and Scialog Research Corporation for Scientific Advancement awards (ST.JOSE and RCSA 28375 and RCSA 28359 to J. J). The funders had no role in study design, data collection and analysis, decision to publish, or preparation of the manuscript.

Competing interests: The authors have declared that no competing interests exist.

Abstract

Flaviviruses such as Zika and dengue viruses are persistent health concerns in endemic regions worldwide. Efforts to combat the spread of flaviviruses have been challenging, as no antivirals or optimal vaccines are available. Prevention and treatment of flavivirus-induced diseases require a comprehensive understanding of their life cycle. However, several aspects of flavivirus biogenesis, including genome packaging and virion assembly, are not well characterized. In this study, we focused on flavivirus capsid protein (C) using Zika virus (ZIKV) as a model to investigate the role of the externally oriented α3 helix (C α3) without a known or predicted function. Alanine scanning mutagenesis of surface-exposed amino acids on C α3 revealed a critical C_{N67} residue essential for ZIKV virion production. The C_{N67A} mutation did not affect dimerization or RNA binding of purified C protein *in vitro*. The virus assembly is severely affected in cells transfected with an infectious cDNA clone of ZIKV with C_{N67A} mutation, resulting in a highly attenuated phenotype. We isolated a revertant virus with a partially restored phenotype by continuous passage of the C_{N67A} mutant virus in Vero E6 cells. Sequence analysis of the revertant revealed a second site mutation in the viral membrane (M) protein M_{F37L}, indicating a genetic interaction between the C and M proteins of ZIKV. Introducing the M_{F37L} mutation on the mutant ZIKV C_{N67A} generated a double-mutant virus phenotypically consistent with the isolated genetic revertant. Similar results were obtained with analogous mutations on C and M proteins of dengue virus, suggesting the critical nature of C α3 and possible C and M residues contributing to virus assembly in other *Aedes*-transmitted flaviviruses. This study provides the first experimental evidence of a genetic interaction between the C protein and the viral envelope protein M, providing a mechanistic understanding of the molecular interactions involved in the assembly and budding of *Aedes*-transmitted flaviviruses.

Author summary

Zika virus and other disease-causing flaviviruses constitute a significant threat to global human health. The development of effective antiviral strategies targeting flaviviruses has

been hindered by a lack of evidence regarding their life cycle, particularly virion assembly. Here, we identified a critical Asn 67 residue in the α3 helix of the C protein mediating ZIKV assembly. We also isolated a compensatory mutation in the M protein, $M_{F37L,}$ that rescues the assembly defect caused by the C_{N67A} mutation, revealing the first evidence of a genetic interaction between C and M protein. Using further molecular genetic analyses, we show that analogous resides in C and M proteins are also required for dengue virus (DENV) assembly, indicating a functional role of this interaction that is conserved among flaviviruses. The data reported here contribute to an increasing collection of evidence pointing toward an interaction between capsid and the external structural proteins of flaviviruses. Our findings describing the genetic interaction between C and M observed in cryo-EM structures but experimentally unproven significantly advance our understanding of *Aedes*-transmitted flavivirus assembly, which will be instrumental in designing assembly-specific flavivirus therapeutics and antivirals.

Introduction

The Flavivirus genus in the *Flaviviridae* family is comprised of more than 70 viruses, including mosquito-borne viruses such as Japanese encephalitis virus (JEV), ZIKV, and dengue virus (DENV), which infects an estimated 100 million people annually, as well as tick-borne viruses like Powassan virus (POWV) and tick-borne encephalitis virus (TBEV). Many flaviviruses cause severe diseases, including hemorrhagic fever, congenital abnormalities, acute flaccid paralysis, and fatal encephalitis in humans [1,2]. A 2022 outbreak of JEV in Australia, infecting swine and causing human fatalities, was declared a communicable disease incident of national significance and is now considered a major global concern [3]. ZIKV gained public interest in 2014 when an epidemic in South America was linked to neurological dysfunction, intrauterine growth retardation, and severe birth defects [4,5]. Vaccination against flaviviruses is also complicated by high mutation rates and immunological factors, including antibody-dependent enhancement; even the currently approved vaccines against West Nile Virus, JEV, and DENV are suboptimal [6–8]. The extensive global spread and epidemic transmission of emerging and reemerging flaviviruses highlights a need for countermeasures targeting structural and functional aspects of virus infection [2].

The functional mechanisms of flavivirus assembly have been determined from the cryo-EM structures of virions and atomic structures of the component proteins [9]. Mature flaviviruses are comprised of an icosahedrally arranged outer shell containing envelope (E) and membrane (M) transmembrane proteins arranged on a host-derived lipid bilayer surrounding an inner core of genomic RNA and C protein [10]. The ~11 kb positive-sense RNA genome encodes a single polyprotein that is processed co-translationally by viral and host proteases into three structural [C, pre-Membrane (prM), and E] and seven non-structural proteins [NS1, NS2A, NS2B, NS3, NS4A, NS4B, and NS5] [11]. The non-structural proteins modify the host endoplasmic reticulum (ER) to form replication factories and vesicle packets similar to other positive-strand RNA viruses and replicate the genomic RNA with a double-stranded RNA intermediate [12–15]. Virus assembly initiates when the positive-strand genomic RNA bound to C protein forms a nucleocapsid, followed by its envelopment by prM and E proteins arranged as trimeric spikes of prM/E heterodimers on the ER membrane and budding into the ER lumen as an immature virus [12]. The 180 prM/E protomers form 60 trimeric spikes that arrange icosahedrally in the immature virus surface lattice, as observed in cryo-EM reconstructions [16,17]. The pr domain capping the fusion loop of E protein is cleaved by host furin

during maturation, which is a pre-requisite for viral infectivity and occurs in the trans-Golgi compartment. The low pH environment of late Golgi induces rearrangement of the trimeric spike into a smooth immature virus structure, allowing the exposure of the furin cleavage site [16–19]. The cleavage of the pr domain by host furin at low pH leads to the stabilization of the smooth mature particle with 90 head-to-tail dimers of M/E in an icosahedral herringbone-like arrangement with cleaved pr still attached to E [20–22]. The mature virus is released into the extracellular milieu via the secretory pathway, and the neutral pH causes the shedding of pr, allowing the virion to mediate acidic pH-triggered membrane fusion upon entry into a new cell [22].

The nucleocapsid organization has not been detected in any mature flavivirus cryo-EM structures, which have resolved the icosahedrally arranged M and E proteins to atomic resolution [10,17,23–25]. However, a partially ordered nucleocapsid shell, including a density connecting the outer envelope to the internal core, has been observed in a 9-Å cryo-EM structure of immature ZIKV and in ~9.5-Å resolution antibody-stabilized structures of DENV and ZIKV [26,27]. Additionally, the presence of a nucleocapsid core was identified from an immature Kunjin virus (KUNV) cryo-EM structure at ~20-Å resolution obtained using asymmetric reconstruction [28]. These immature virus structures were generated using viruses purified from ammonium chloride-treated cells that did not encounter low pH in the late Golgi [29]. It is interesting to note that core density is not observed in the 7.8-Å resolution cryo-EM structure of immature Spondweni virus (SPOV) and 4.4-Å cryo-EM structure of Binjari virus (BinJV), which were both determined using immature virus particles selected from mature virus preparations [16,17]. Therefore, it is conceivable that there are transient interactions between C and prM/E proteins in the immature virus, which are possibly lost during virus maturation, leading to a rearrangement of the nucleocapsid core in the mature virions.

Despite currently available high-resolution structures of mature and immature flaviviruses, the mechanism of nucleocapsid formation and interactions of C protein with the viral envelope leading to virus assembly and budding are not well understood. Although hydrophobic interactions between the membrane-anchored prM/E proteins and the nucleocapsid that mediate virus assembly have been proposed, finding evidence for this link has been challenging due to the likely transient nature of potential interactions [2,26,27]. Transmembrane domains of E protein have been shown to contribute to the formation of nucleocapsid integration into the budding viral envelope in TBEV assembly [30]. Similarly, using the cryo-EM structure of ZIKV and structure-based mutagenesis, we have previously identified a conserved W474 residue on the E transmembrane domain interacting with the lipid pocket factor required for ZIKV assembly [31]. Interactions between prM and E are sufficient for budding as virus-like particles can be produced from the expression of prM and E, and subviral particles containing only prM and E are regularly found during virus infection [32–34]. Therefore, the mechanism orchestrating the nucleocapsid incorporation into budding virus particles remains undetermined, exacerbated by the lack of data regarding the C protein region involved in the formation of the nucleocapsid core that packages the viral genomic RNA. Furthermore, a packaging signal has not been detected in flavivirus genomic RNA, and the proposed interactions between C protein and genomic RNA occur in a nonspecific manner through electrostatic interactions [35]. Flavivirus assembly is also tightly coupled to RNA replication, with electron tomography studies showing nucleocapsid formation and virus budding into the ER lumen occur in close proximity to the RNA exit sites of replication vesicles in the ER [12–14]. Evidence supporting a replication-coupled assembly mechanism in flaviviruses has been obtained from non-structural protein NS2A interacting with the 3′ untranslated region (UTR) and has been proposed as an assembly chaperone that may provide the specificity for genome RNA packaging [9,36–38]. Although mutagenesis studies have characterized critical C protein

residues in RNA binding, dimerization, and lipid droplet binding, thus far, a specific budding defective C protein mutation has not been identified to implicate a C protein region involved in virion formation [39–41].

The X-ray crystal and NMR structures of flavivirus C proteins expressed and purified from bacteria have shown the structure as a homodimer, with each monomer consisting of four α-helices (α1–α4) and an intrinsically disordered N-terminal region that remains unresolved [22,42–46]. The ZIKV C protein is a small 104 amino acid protein, and the structure of residues 23–98 has been determined by both X-ray crystallography and NMR [43,45]. The first alpha helix α1 (residues 37–40) forms the top level of the protein, alpha helices α2 (residues 44–56) and α3 (residues 63–71) and their connecting loop forms the middle layer, and alpha helix α4 (residues 74–97) which is oriented perpendicular to the α3 helix forms the bottom layer. The C protein dimerization is mediated by interactions of antiparallel α2 and α4 helices of the two subunits. There is a hydrophobic cleft between α1 and α2 helices in the C dimer, which has been proposed to interact with the membranes; however, this cleft is obstructed by the unstructured N-terminal domain in ZIKV [42,43]. The α4 helix contains several positively charged residues that are proposed to interact with RNA [47,48].

While several studies have characterized the structural importance of α1, α2, and α4 helices of flavivirus C protein [39,40,49,50], as well as the transmembrane anchor helix α5 [27], few have focused on the importance of the α3 helix, which forms the outer edge of the C protein and contains multiple surface-exposed residues in the dimeric structure. In this study, we determined that the α3 helix of ZIKV C protein is critical for virus assembly and budding, replacing a surface-exposed residue C_{N67} from the α3 with alanine inhibited virus production without affecting dimerization or RNA binding *in vitro*. We identified a second site compensatory mutation in the M protein, M_{F37L}, which rescues the lethal phenotype of the C_{N67A} mutant. Further mutational analyses of DENV and characterization of DENV residues C_{K67} and M_{L37} in structurally similar positions in C α3 and M proteins revealed a significant reduction in virus titer and plaque sizes, confirming the importance of these residues across *Aedes*-transmitted flaviviruses. This study demonstrates the critical role of α3 in virus assembly and provides the first evidence for a genetic interaction of C protein with a membrane-anchored structural protein in mediating virus budding, a crucial step in flavivirus morphogenesis.

Results

Alanine scanning of C α3 identifies asparagine 67 as a critical residue for ZIKV production

The primary role of C protein in flavivirus biogenesis is genome packaging. Of the four α helices that comprise the C protein (α1–4), the predicted functions for α1, α2, and α4 include lipid binding, dimerization, and RNA binding, respectively [35,39,40]. In contrast, the role of the α3 helix remains poorly understood. Here, we investigated the functional role of α3 in mediating virus assembly and virion morphogenesis by mutational and biochemical analyses. Alanine substitutions were introduced by site-directed mutagenesis on ZIKV containing a fluorescently tagged NS2A ($ZIKV_{venus}$), which enabled us to measure virus spread by fluorescence microscopy (Fig 1A). We selected C protein residues I66, N67, R68, and S71 from the α3 for mutagenesis based on the side chain orientation and surface exposure from the ZIKV C crystal structure (PDB:5YGH, Fig 1B) and NMR structure (PDB:6C44). We generated a quadruple alanine substitution [$_{66}$INRWGS$_{71}$/$_{66}$AAAWGA$_{71}$ ($ZIKV_{venus}$-Cm)] as well as individual alanine substitutions $ZIKV_{venus}$-C_{I66A}, $ZIKV_{venus}$-C_{N67A}, $ZIKV_{venus}$-C_{R68A}, and $ZIKV_{venus}$-C_{S71A}. Individual alanine substitution sequences were analyzed by AlphaFold, which predicted structures similar to WT ZIKV C for all four mutants (S1 Fig) [51]. The wild-type and mutant

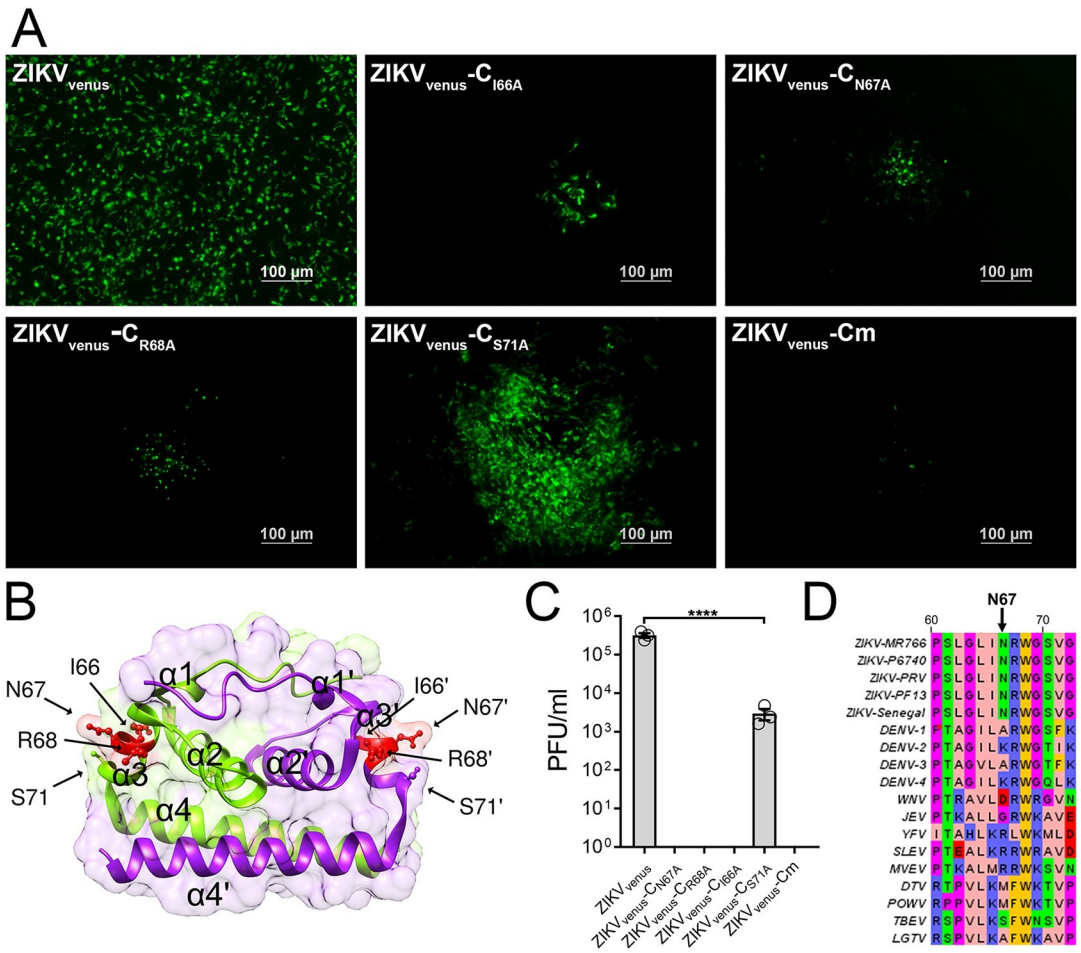

Fig 1. Mutational analysis of ZIKVC α3. (A) Micrographs showing fluorescent clusters of Vero E6 cells infected with wild-type ZIKV$_{venus}$ or ZIKV$_{venus}$ containing mutant C protein I66A(ZIKV$_{venus}$-C$_{I66A}$), N67A(ZIKV$_{venus}$-C$_{N67A}$), R68A(ZIKV$_{venus}$-C$_{R68A}$), S71A(ZIKV$_{venus}$-C$_{S71A}$), and combination mutant INRWSG/AAAWAG (ZIKV$_{venus}$-Cm), showing virus spread. Images were acquired at 5 d.p.i. (B) The crystal structure of ZIKV C dimer (PDB:5YGH) was generated using UCSF Chimera software. Chain A is green, and chain B is purple with α1–4 labeled on the structure. Residues selected for mutational analysis are depicted as ball and stick. (C) Virus titers of wild-type and mutant ZIKV$_{venus}$ (passage 0) as determined by plaque assay in Vero E6 cells. Column labels correspond to viruses in (A). The graph represents average titers (n = 3) with error bars representing the standard error of the mean (SEM). Statistical significance was calculated by Ordinary one-way ANOVA using GraphPad PRISM 7 software at a 95% confidence interval. Relative significance is indicated by asterisks ($p<0.0001$ = ****). (D) Sequence alignment of flavivirus C α3 helices with the residue of interest N67 denoted by an arrow above. Sequence accession numbers [ZIKV MR766: AMR39835.1, ZIKV P6740: AVK43549.1, ZIKV PRV: AMC13911.1, ZIKV PF13: ARB08112.1, ZIKV Senegal: AMR39832.1, DENV 1: ADK37471.1, DENV 2: NP_056776.2, DENV 3: ABW82020.1, DENV 4: ARM59249.1, WNV: Q9Q6P4.2, JEV: NP_059434.1, YFV: NP_041726.1, SLEV: YP_001008348.1, MVEV: NP_051124.1, DTV: AAL32169.1, POWV: NP_620099.1, TBEV: ABI 31771.1, LGTV: QBR53298.1].

https://doi.org/10.1371/journal.pntd.0011873.g001

ZIKV$_{venus}$ clones were transfected into HEK 293-T cells, and cell culture supernatants were collected after 4 days. We infected Vero E6 cells with the collected supernatants to visualize phenotypic differences in virus spread based on fluorescent cell cluster sizes at 5 days post infection (d.p.i). (Fig 1A). In cells infected with ZIKV$_{venus}$, we observed large foci containing >200 fluorescent cells. In contrast, the ZIKV$_{venus}$-C$_{I66A}$, ZIKV$_{venus}$-C$_{N67A}$, and ZIKV$_{venus}$-C$_{R68A}$ mutant viruses formed very few, small fluorescent foci containing approximately 10–20 cells, and the ZIKV$_{venus}$-C$_{S71A}$ mutant virus formed large fluorescent clusters of >100 cells (Fig 1A). The ZIKV$_{venus}$-Cm mutant was severely attenuated, with very few cells expressing

green fluorescence and no observable spread from cell to cell. We further estimated the virus titer from the supernatants of transfected cells by plaque assay in Vero E6 cells (Fig 1C). Wild-type $ZIKV_{venus}$ had an average titer of 3.20×10^5 PFU/ml, and the $ZIKV_{venus}$-C_{S71A} mutant virus was ~2 log lower with an average titer of 2.93×10^3 PFU/ml. In contrast, the virus mutants $ZIKV_{venus}$-C_{I66A}, $ZIKV_{venus}$-C_{N67A}, and $ZIKV_{venus}$-C_{R68A} did not form observable plaques, suggesting that these three residues on α3 are essential for virus production. $ZIKV_{venus}$-Cm was also non-plaque forming. In the structure of ZIKV C, N67 appears significantly more solvent accessible than I66 and R68 (Fig 1B); therefore, we selected C_{N67} as our residue of interest for further studies. Intriguingly, even though C_{N67} residue is conserved among different strains of ZIKV, it is less conserved among other *Aedes*-transmitted flaviviruses when compared to C_{I66} and C_{R68} residues (Fig 1D).

N67A mutation of ZIKV C does not affect oligomerization or RNA binding *in vitro*

To test whether attenuation of the $ZIKV_{venus}$-C_{N67A} mutant virus was due to C protein defects that cause inability to fold properly, dimerize, or bind nucleic acids, we expressed wild-type (MBP-C_{WT}) and N67A mutant (MBP-C_{N67A}) C proteins as N-terminal MBP fusion proteins in bacteria which were then purified by affinity chromatography using an amylose resin followed by Hi-Trap Heparin column. Both MBP-C_{WT} and MBP-C_{N67A} proteins were stable and purified to homogeneity as determined by Size Exclusion Chromatography (S2 Fig), with a molecular weight of 54 kDa as determined by SDS-PAGE (Fig 2A). We then evaluated whether the C_{N67A} mutation influenced capsid-RNA binding *in vitro* by performing an Electrophoretic Mobility Shift Assay (EMSA) (Fig 2B). Both MBP-C_{WT} and MBP-C_{N67A} proteins showed a concentration-dependent binding to RNA representing the 5'UTR and C gene of ZIKV; we observed a shift in the RNA band towards a higher molecular weight RNA+C protein complex in correlation with an increasing ratio of protein to RNA. We next tested if the C_{N67A} mutation affects the oligomerization of C protein by glutaraldehyde (GA) crosslinking (Fig 2C). At a lower concentration of GA (0.25 mM), both MBP-C_{WT} and MBP-C_{N67A} formed dimer (>100 kDa) as well as higher order oligomers, possibly tetramers. At higher concentrations of GA (0.5 and 1.0 mM), both proteins are oligomerized to possible tetramers (>200 kDa). These data indicate that MBP-C_{WT} and MBP-C_{N67A} have similar oligomerization properties (Fig 2C). Taken together, our results prove that the C_{N67A} mutation does not affect the RNA binding and oligomerization properties of the C protein.

N67A mutation does not alter the intracellular distribution of ZIKV C protein in mammalian cells

In flavivirus-infected cells, C protein localizes to the ER and lipid droplets (LD) with functional implications for virus assembly [39,40]. The C protein also localizes to the nucleolus, although the importance of this phenomenon is not yet understood [40,41]. We tested whether C_{N67A} affects the localization of C to LD or the nucleolus by ectopic expression of N-terminal mCherry tagged C proteins (mCherry-C_{WT} and mCherry-C_{N67A}) in JEG-3 cells followed by live confocal microscopy. In cells stained with MDH for LD visualization, mCherry-C_{WT} (Fig 3A) and mCherry-C_{N67A} (Fig 3B) were observed localizing to the surface of LD, suggesting that both C proteins interact with the LD membrane. We then co-expressed mCherry-tagged C protein with GFP tagged nucleolin, a nucleolar marker, in JEG-3 cells. We observed clear colocalization of both mCherry-C_{WT} (Fig 3C) and mCherry-C_{N67A} (Fig 3D) with GFP-nucleolin.

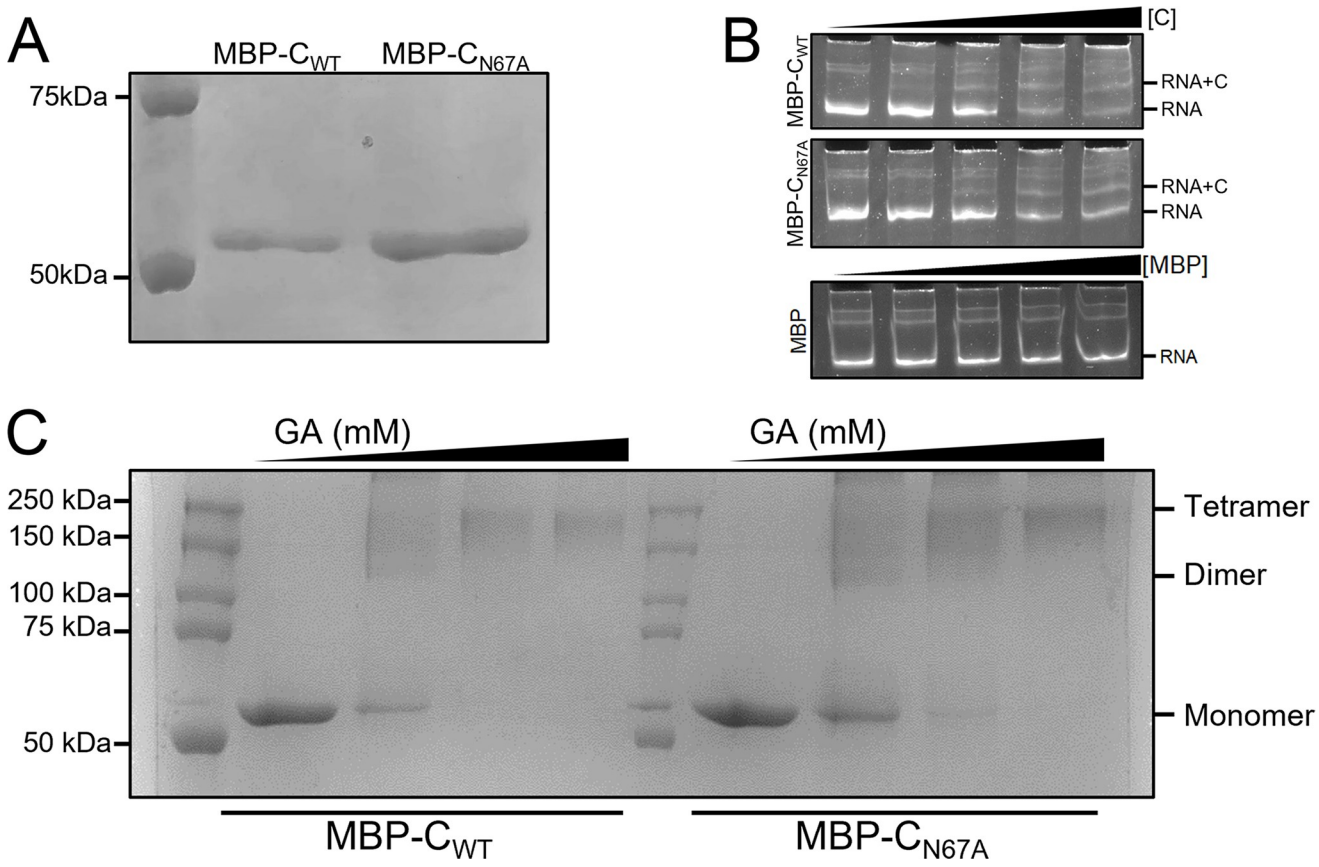

Fig 2. Biochemical characterization of WT and N67A mutant C proteins. Wild-type (MBP-C_{WT}) and N67A mutant (MBP-C_{N67A}) C were expressed and purified as MBP fusion proteins. (A) SDS-PAGE gel showing the purified MBP-C_{WT} and MBP-C_{N67A}. (B) EMSA showing binding of MBP-C_{WT} (top panel), MBP-C_{N67A} (middle panel), or MBP alone (bottom panel) to RNA representing 5'UTR and C gene of ZIKV. Relative molar ratios of RNA: protein are indicated by the triangle above, from left to right: 1:0, 1:1.5, 1:3, 1:6, 1:9. (C) SDS-PAGE of samples from glutaraldehyde (GA) crosslinking assay. Samples from MBP-C_{WT} and MBP-C_{N67A} after 20 min crosslinking reaction. Relative GA concentrations are indicated by triangles above, from left to right: 0 mM, 0.25 mM, 0.5 mM, 1.0 mM. The size of the C-MBP monomer, dimer, and possible tetramer is indicated on the right.

https://doi.org/10.1371/journal.pntd.0011873.g002

C_{N67A} mutant virus has a significant defect in ZIKV assembly

We next tested whether N67A mutation causes defects in the assembly or replication of ZIKV-$_{venus}$ in JEG-3 cells by immunofluorescence (IF) analysis for C localization to Golgi (Fig 4A–4C) and dsRNA production (Fig 4D–4F), respectively. In these experiments, we used cells transfected with plasmids encoding wild-type $ZIKV_{venus}$, $ZIKV_{venus}$-$C_{N67A,}$ or an assembly deficient control $ZIKV_{venus}$-$C_{K85A/K86A}$ viruses, all expressing venus-NS2A protein (green) [40]. When $ZIKV_{venus}$ transfected cells were probed with an anti-giantin antibody as a Golgi marker (magenta) and an anti-ZIKV C antibody (red), we observed C protein localizing to ER and Golgi (Fig 4A). In $ZIKV_{venus}$-C_{N67A} and $ZIKV_{venus}$-$C_{K85A/K86A}$ transfected cells, C protein is found localized to the ER but less on the Golgi compared to the wild-type C protein (Fig 4B and 4C). Pearson's correlation coefficient analysis of $ZIKV_{venus}$ infected cells showed an average value of 0.625±0.147 for the colocalization of C protein with Golgi (Fig 4G). In contrast, cells transfected with $ZIKV_{venus}$-C_{N67A} showed an average value of 0.108±0.068 suggesting a significantly reduced colocalization of C protein with Golgi, much like the assembly deficient control $ZIKV_{venus}$-$C_{K85A/K86A}$ which showed an average value of 0.169±0.076. To determine if the inability to assemble is a byproduct of a replication defect, we probed $ZIKV_{venus}$, $ZIKV_{venus}$-C_{N67A}, or $ZIKV_{venus}$-$C_{K85A/K86A}$ transfected cells for the presence of dsRNA using dsRNA

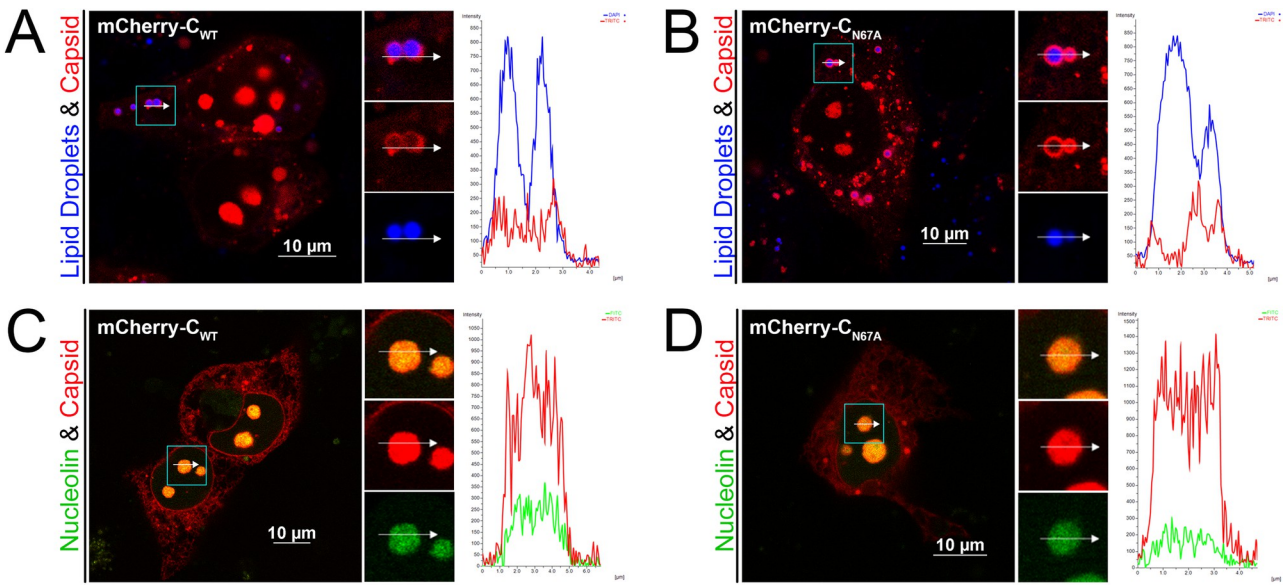

Fig 3. Colocalization of WT and N67A mutant C protein to lipid droplets and nucleolus. N-terminal mCherry tagged WT (mCherry-C_{WT}) and N67A mutant (mCherry-C_{N67A}) C proteins were expressed in JEG-3 cells, and their colocalization to LD and nucleolus were determined by confocal microscopy. (A-B) Fluorescent micrographs of JEG-3 cells transfected with mCherry-C_{WT} (A) or mCherry-C_{N67A} (B) and stained with MDH for LD (blue). (C-D) Fluorescent micrographs of JEG-3 cells co-expressing mCherry-C_{WT} (C) or mCherry-C_{N67A} (D) with nucleolar maker GFP-nucleolin. Regions of interest (ROI) are marked and represented as zoomed images to the right in separate channels. Line graphs to the right of each image show the relative intensity of red and blue (A-B) or red and green (C-D) channels corresponding to the white arrow inside the ROI. All images were acquired at 24 h.p.t.

https://doi.org/10.1371/journal.pntd.0011873.g003

specific antibody (Fig 4D–4F). Distinct dsRNA-associated foci (magenta) were observed throughout the cells in all samples, confirming that replication is unaffected by mutation of C_{N67A} or $C_{K85A/K86A}$. The assembly defect of ZIKV$_{venus}$-$C_{N67A,}$ as inferred from the IF analysis, was further verified by qRT-PCR and western blot to evaluate viral genomic RNA and virus particles released from cells, respectively. Intact virus particles released from cells were harvested from the cell culture supernatants by ultracentrifugation using a sucrose cushion, and RNA molecules were quantified by qRT-PCR (Fig 4H). In wild-type ZIKV$_{venus}$ samples, we detected an average of 2.37×10^7 RNA molecules/ml. The number of molecules detected in ZIKV$_{venus}$-C_{N67A} samples was ~2 log lower at an average of 1.74×10^5 RNA molecules/ml, similar to the assembly deficient control ZIKV$_{venus}$-$C_{K85A/K86A,}$ which gave an average value of 6.69×10^4 RNA molecules/ml. A second aliquot of the purified virus pellet obtained by ultracentrifugation was used to detect the presence of C protein via western blot using an anti-ZIKV C antibody (Fig 4I). A band corresponding to the cleaved C monomer at <20 kDa was observed for ZIKV$_{venus}$. In comparison, no detectable C band was observed in ZIKV$_{venus}$-$C_{N67A,}$ similar to the negative controls purified from ZIKV$_{venus}$-$C_{K85A/K86A}$ and mock-infected cells.

ZIKV C tolerates a positively charged residue at position 67 but not hydrophobic residues

To test the importance of asparagine residue at the 67th position of C protein, which is conserved in all ZIKV strains but not in other flaviviruses, we replaced the N67 with G and K based on mosquito-borne flaviviruses JEV and DENV-2 sequences of C protein, and to M and R based on tick-borne flaviviruses DTV and POWV C protein sequences. We also substituted the hydrophilic N67 with a hydrophobic amino acid L. Cell culture supernatants of ZIKV$_{venus}$

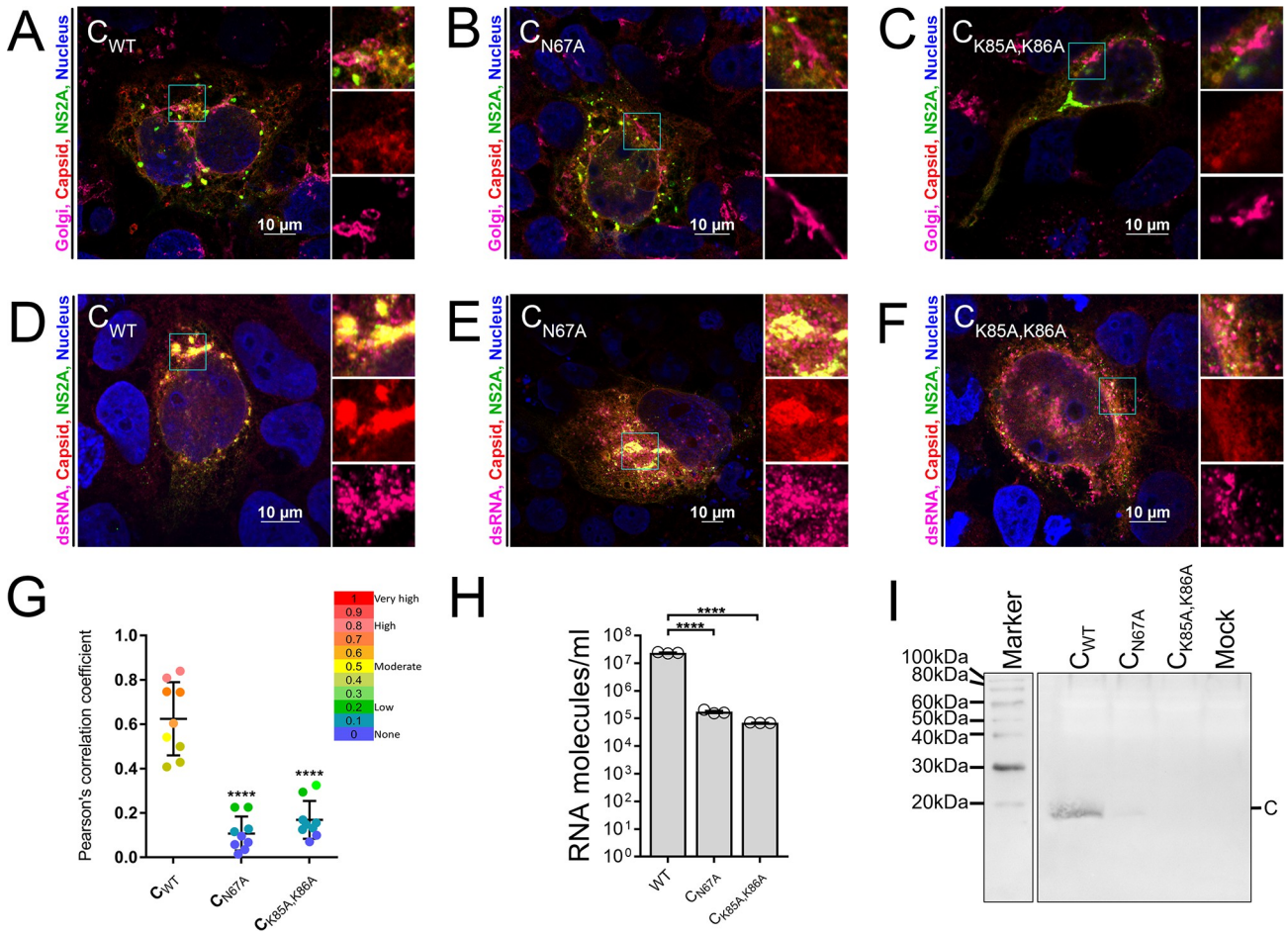

Fig 4. Effect of C N67A mutation on ZIKV assembly and replication. JEG-3 cells were transfected with full-length cDNA clones of WT ZIKV$_{venus}$ (A, D) ZIKV$_{venus}$-C$_{N67A}$ (B, E) or C assembly negative control mutant K85A/K86A (ZIKV$_{venus}$-C$_{K85A/K86A}$) (C, F). Permeabilized cells were probed with antibodies against C (red) and Golgi marker Giantin (magenta) to determine the localization of C protein to the Golgi apparatus (A-C) or anti-dsRNA antibody (magenta) to detect replicating viral RNA (D-F). All cells were stained with Hoechst (blue) to detect the nucleus. The green color represents venus-tagged NS2A translated from the viral RNA. ROIs are outlined in cyan and represented as zoomed images to the right in separate channels. (G) Pearson's correlation coefficients were calculated for the colocalization of C protein and Golgi using Nikon NIS Elements software. ROIs containing Golgi were selected from the confocal micrographs for each virus for calculation. Data points represent Pearson's correlation coefficient (n = 9), with error bars representing mean and standard deviation (SD). Statistical significance was calculated by Ordinary one-way ANOVA using PRISM software at a 95% confidence interval. Relative significance is indicated by asterisks ($p<0.0001$ = ****). The heatmap indicates the colocalization range, and the data points are colored accordingly. (H-I) Detecting release of assembled virus in culture supernatants by qRT-PCR (H) and Western blot (I) 48 h.p.i. (H) Number of RNA molecules per ml of cell culture supernatant estimated by qRT-PCR. The number of RNA molecules/ml was calculated based on the Ct standard curve generated from ZIKV genomic RNA of a known quantity. The graph represents average RNA molecules/ml (n = 3) with error bars representing SEM. Statistical significance was calculated by Ordinary one-way ANOVA using GraphPad PRISM 7 software at a 95% confidence interval. Relative significance is indicated by asterisks ($p<0.0001$ = ****). Graph normalized to mock infected samples. (I) Western blot represents virus pellets obtained after ultracentrifugation of the cell culture supernatants probed with anti-ZIKV C antibody. Label C on the right indicates a band corresponding to the released ZIKV C protein.

https://doi.org/10.1371/journal.pntd.0011873.g004

with the introduced mutations were harvested and used to infect Vero E6 cells. After 5 days, cells were analyzed by fluorescence microscopy for the formation of fluorescent cell clusters representing virus spread (Fig 5A). Wild-type ZIKV$_{venus}$ formed large clusters of >200 fluorescent cells, whereas ZIKV$_{venus}$-C$_{N67A,}$ ZIKV$_{venus}$-C$_{N67M,}$ and ZIKV$_{venus}$-C$_{N67L}$ mutant viruses all formed small foci containing 10–20 fluorescent cells. The ZIKV$_{venus}$-C$_{N67G}$ mutant virus did not form observable fluorescent cell clusters. ZIKV$_{venus}$-C$_{N67R}$ formed clusters with 30–50 cells, and ZIKV$_{venus}$-C$_{N67K}$ formed large clusters with an average of ~100 cells. The ZIKV$_{venus}$-

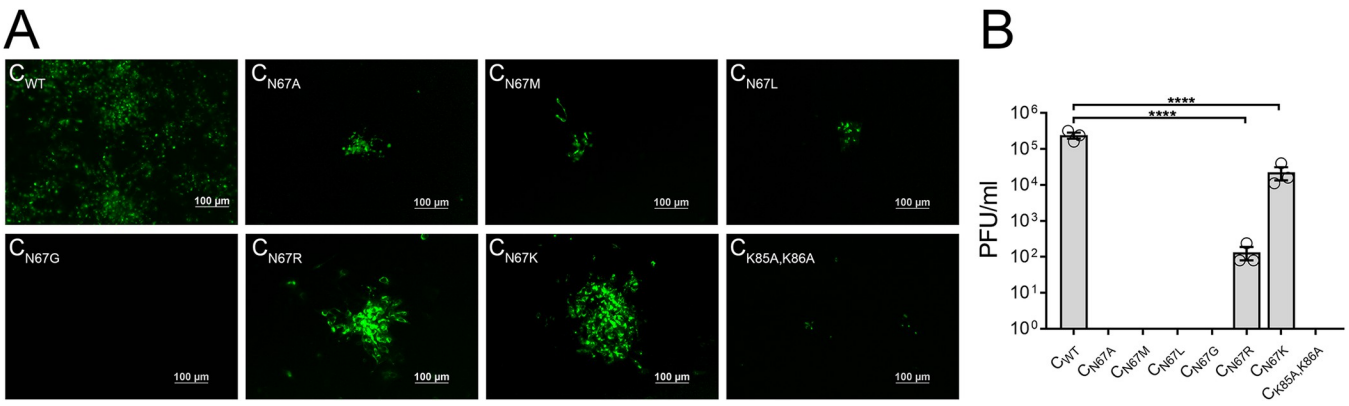

Fig 5. Amino acid substitution of C residue 67. (A) Micrographs showing fluorescent clusters of Vero E6 cells infected with WT $ZIKV_{venus}$ or C mutant viruses $ZIKV_{venus}$-C_{N67A}, N67M($ZIKV_{venus}$-C_{N67M}), N67G($ZIKV_{venus}$-C_{N67G}), N67L($ZIKV_{venus}$-C_{N67L}), N67R($ZIKV_{venus}$-C_{R67R}), N67K($ZIKV_{venus}$-C_{R67K}), and negative control mutant $ZIKV_{venus}$-$C_{K85A/K86A}$, demonstrating relative virus spread. Images were acquired at 5 d.p.i. (B) Virus titers of wild-type and mutant $ZIKV_{venus}$ as determined by plaque assay in Vero E6 cells. The graph represents average titers (n = 3) with error bars representing SEM. Statistical significance was calculated by Ordinary one-way ANOVA using GraphPad PRISM 7 software at a 95% confidence interval. Relative significance is indicated by asterisks ($p<0.0001$ = ****).

https://doi.org/10.1371/journal.pntd.0011873.g005

$C_{K85A/K86A}$ assembly mutant was used as a negative control for this assay, which showed highly attenuated cluster formation. Cell culture supernatants were also analyzed to determine virus titer by plaque assay (Fig 5B). $ZIKV_{venus}$ had a titer of 3.20×10^5 PFU/ml. Mutant viruses that formed very small or no clusters ($ZIKV_{venus}$-C_{N67A}, $ZIKV_{venus}$-C_{N67M}, $ZIKV_{venus}$-C_{N67L}, and $ZIKV_{venus}$-C_{N67G}) were all non-plaque forming and showed no measurable titer. $ZIKV_{venus}$-C_{N67K} had sizeable fluorescent cell clusters, and $ZIKV_{venus}$-C_{N67R}, which showed 25–30 cell clusters, gave significantly reduced titers of 1.33×10^2 and 2.24×10^4 PFU/ml, respectively.

A second site reversion in M protein rescues ZIKV-C_{N67A}

Even though the C_{N67A} mutant virus is severely attenuated, the mutant provided the opportunity to screen for revertants that rescue the phenotype. We used the fluorescent $ZIKV_{venus}$-C_{N67A} virus collected from transfected HEK-293T cells (P0) to infect Vero E6 cells in triplicate. After 6 days, supernatants were collected and passaged consecutively up to five times in Vero E6 cells. Cells were monitored for the emergence of sizeable fluorescent cell clusters indicating rescued phenotype. After five passages (P5), large fluorescent groups containing >100 cells per cluster were observed in all three replicates (Fig 6A). We performed RT-PCR on the P5 supernatant to amplify the gene encoding C, followed by Sanger sequencing of the amplicons. Out of three replicates, two had reverted to wild-type $ZIKV_{venus}$-C_{N67}, and the third retained the C_{N67A} mutation. To further analyze this third replicate, we performed RT-PCR and Sanger sequencing of genes encoding prM and E structural proteins, revealing a single nucleotide second site mutation in M protein changing F37 to L37 ($ZIKV_{venus}$-C_{N67A}+M_{F37L}) (Fig 6B). To confirm the rescue of phenotype by C_{N67A}+M_{F37L}, we compared its titer with the titers of $ZIKV_{venus}$-C_{N67A} and wild-type $ZIKV_{venus}$ obtained by plaque assay. While $ZIKV_{venus}$-C_{N67A} did not form plaques, $ZIKV_{venus}$-C_{N67A}+M_{F37L} had an average titer of 2.4×10^4 PFU/ml compared to $ZIKV_{venus}$ which gave an average tier of 4.53×10^5 PFU/ml (Fig 6C). Next, to confirm the M_{F37L} mutation alone rescues the attenuated phenotype of ZIKV-C_{N67A}, we engineered non-fluorescent ZIKV ($ZIKV_{WT}$) cDNA to obtain viruses containing C_{N67A} ($ZIKV_{WT}$-C_{N67A}) single mutation and C_{N67A}+M_{F37L}($ZIKV_{WT}$-C_{N67A}+M_{F37L}) double mutations. We then compared the growth kinetics of $ZIKV_{WT}$-C_{N67A}+M_{F37L} with $ZIKV_{WT}$ in Vero E6 cells (Fig 6D). Cell culture supernatants had comparable virus titers at 96 h.p.i. The $ZIKV_{WT}$-C_{N67A}+M_{F37L}

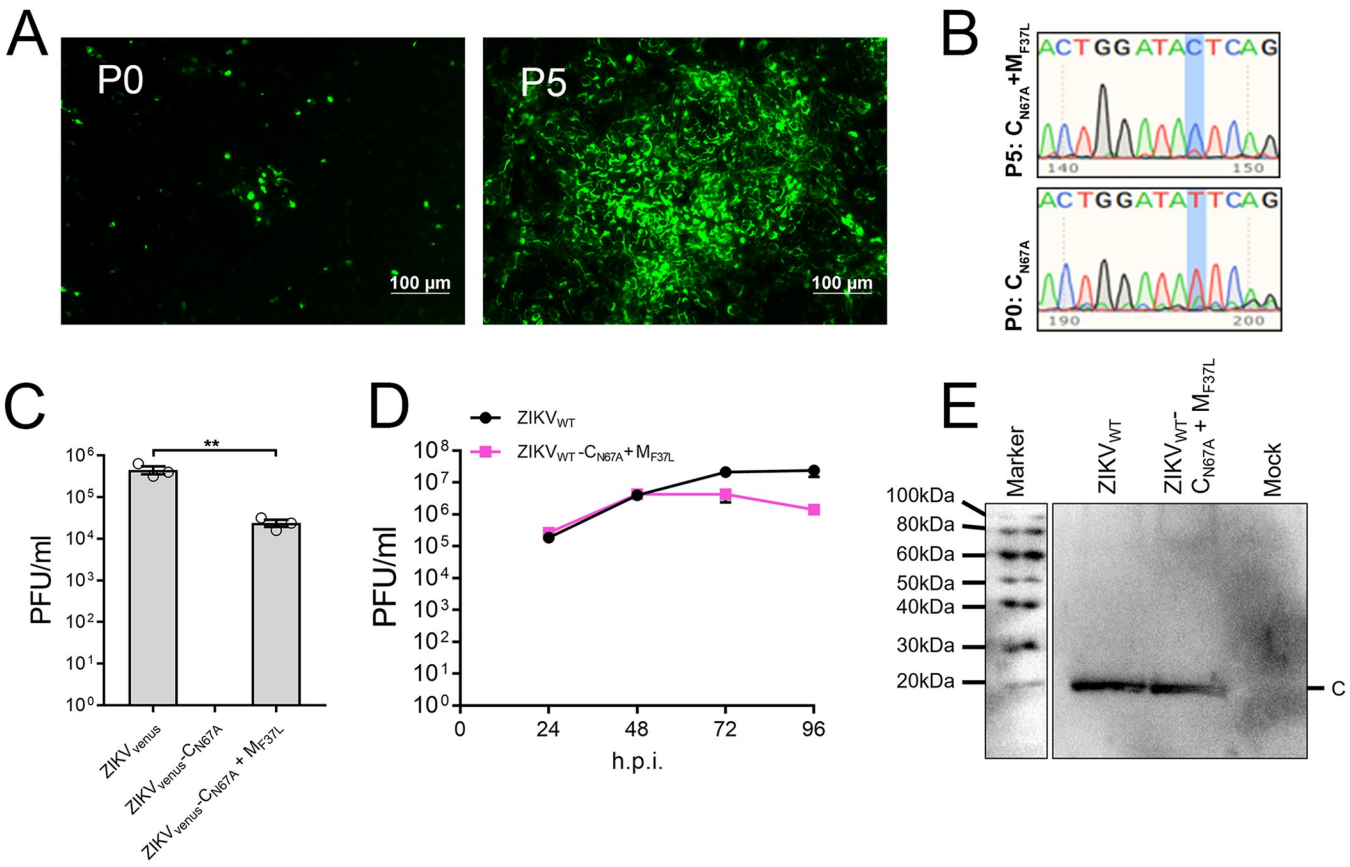

Fig 6. Identification and characterization of C_{N67A}+M_{F37L} revertant. (A) Micrographs showing fluorescent clusters of Vero E6 cells infected with $ZIKV_{venus}$-C_{N67A} at passage 0 (P0) and passage 5 (P5). (B) Sanger sequencing results analyzed using FinchTV software showing the region of mutation in M protein in the P5 revertant virus. A single nucleotide T→C mutation (highlighted in blue) created an F→L amino acid mutation in the M protein resulting in a $ZIKV_{venus}$-C_{N67A+}+M_{F37L} double mutant. (C) Virus titers of $ZIKV_{venus}$-C_{N67A} mutant and $ZIKV_{venus}$-C_{N67A+}+M_{F37L} revertant compared to wild-type $ZIKV_{venus}$ as determined by plaque assay on Vero E6 cells. The graph represents average titers (n = 3) with error bars representing SEM. Statistical significance was calculated by Ordinary one-way ANOVA using GraphPad PRISM 7 software at a 95% confidence interval. Relative significance is indicated by asterisks ($p<0.01$ = **). (D) Growth curve analysis of $ZIKV_{WT}$ and $ZIKV_{WT}$-C_{N67A+}+M_{F37L}. The graph represents average titers (n = 3) at 24-, 48-, 72-, and 96 h.p.i with error bars representing SEM. (E) Western blot of virus pellets obtained after ultracentrifugation of the cell culture supernatants probed with anti-ZIKV C antibody. Label -C on the right indicates a band corresponding to the ~~released~~ ZIKV C protein.

https://doi.org/10.1371/journal.pntd.0011873.g006

reached an average titer of 1.41×10^6 PFU/ml, compared to $ZIKV_{WT,}$ which gave an average titer of 2.42×10^7 PFU/ml. To confirm the assembly and release of $ZIKV_{WT}$-C_{N67A}+M_{F37L} from infected cells, we purified the virus from supernatants of infected Vero E6 cells and performed western blot analysis using an anti-ZIKV C antibody. A band corresponding to ZIKV C was observed near <20 kDa in $ZIKV_{WT}$ and double mutant $ZIKV_{WT}$-C_{N67A}+M_{F37L} samples, confirming virus release (Fig 6E).

The amino acid at position 37 of M significantly impacts the ZIKV virus life cycle

In the cryo-EM structure of mature ZIKV M/E heterodimer (PDB:6CO8), $M_{F37,}$ which reverted to L and rescued the C_{N67A} mutant, is located on the first perimembrane helix of M (M-H1) near the outer leaflet of the lipid bilayer that makes up the viral membrane (Fig 7A) [10]. M_{F37} is not a highly conserved residue, although the phenylalanine is conserved within ZIKV strains, and relative hydrophobicity is conserved across flaviviruses (Fig 7B). To evaluate

the significance of the residue at position 37 in ZIKV M, we generated a $ZIKV_{venus}$-M_{F37A} mutant by site-directed mutagenesis. We also included $ZIKV_{venus}$-M_{F37I}, $ZIKV_{venus}$-M_{F37W}, and $ZIKV_{venus}$-M_{F37L}, to analyze the effect of analogous residues found in related flaviviruses JEV, DENV, and POWV, respectively. Mutations were first introduced into $ZIKV_{venus}$, and virus production was estimated by plaque assay of cell culture supernatants. Wild-type $ZIKV_{venus}$ had an average titer of 5.6×10^5 PFU/ml, whereas F37A substitution was lethal, strongly suggesting that F37 is a critical residue for viral production (Fig 7C). $ZIKV_{venus}$-M_{F37W} was attenuated, producing a titer of 3.20×10^3 PFU/ml. $ZIKV_{venus}$-M_{F37I} and $ZIKV_{venus}$-M_{F37L} resulted in high virus titers of 4.8×10^5 PFU/ml and 9.07×10^5 PFU/ml, respectively, showing

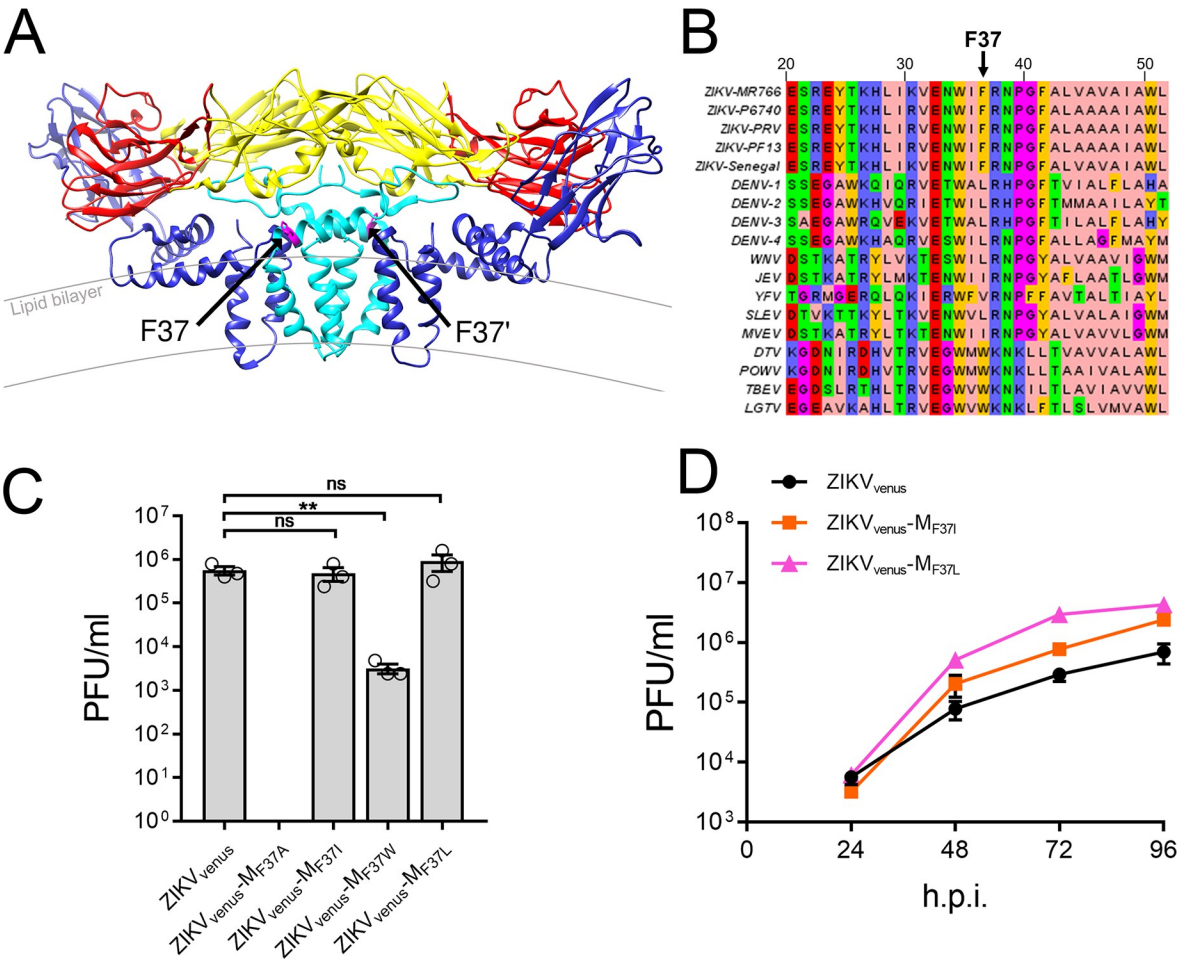

Fig 7. Mutational analysis of ZIKV M residue 37. (A) Cryo-EM structure of mature ZIKV M/E heterodimers (PDB:6CO8) showing the position of M_{F37} residue in magenta and marked with black arrows. E protein chains are shown with standard domain coloring (domain I: red, domain II: yellow, domain III: blue), and M protein chains are represented in cyan. The lipid bilayer is indicated by curved gray lines. (B) Multiple sequence alignment of flavivirus M perimembrane helix (M-H1) annotated in Jalview with Zappo coloring. The residue of interest F37 is denoted by an arrow above. Sequence accessions numbers [ZIKV MR766: AMR39835.1, ZIKV P6740: AVK43549.1, ZIKV PRV: AMC13911.1, ZIKV PF13: ARB08112.1, ZIKV Senegal: AMR39832.1, DENV 1: ADK37471.1, DENV 2: NP_056776.2, DENV 3: ABW82020.1, DENV 4: ARM59249.1, WNV: Q9Q6P4.2, JEV: NP_059434.1, YFV: NP_041726.1, SLEV: YP_001008348.1, MVEV: NP_051124.1, DTV: AAL32169.1, POWV: NP_620099.1, TBEV: ABI 31771.1, LGTV: QBR53298.1] (C) Virus titers (passage 0) calculated from plaque assay of $ZIKV_{venus}$, and M_{37} substitution mutant viruses F37A($ZIKV_{venus}$-M_{F37A}), F37I($ZIKV_{venus}$-M_{F37I}), F37W($ZIKV_{venus}$-M_{F37W}), and F37L($ZIKV_{venus}$-M_{F37L}). The graph represents average titers (n = 3) with error bars representing SEM. Statistical significance was calculated by Ordinary one-way ANOVA using GraphPad PRISM 7 software at a 95% confidence interval. Relative significance is indicated by asterisks ($p<0.01$ = **, $p>0.05$ considered not significant (ns)). (D) Growth curve analysis of $ZIKV_{venus}$, $ZIKV_{venus}$-M_{F37I}, and $ZIKV_{venus}$-M_{F37L} viruses. The graph represents average titers (n = 3) at 24-, 48-, 72-, and 96 h.p.i with error bars representing SEM.

https://doi.org/10.1371/journal.pntd.0011873.g007

that these mutations are tolerated in ZIKV (Fig 7C). We next compared the growth kinetics of the mutants $ZIKV_{venus}$-M_{F37L} and $ZIKV_{venus}$-M_{F37I} with wild-type $ZIKV_{venus}$ (Fig 7D). $ZIKV_{venus}$-M_{F37W} was not included in this assay due to its reduced titer. Both $ZIKV_{venus}$-M_{F37L} and $ZIKV_{venus}$-M_{F37I} resulted in titers that exceeded $ZIKV_{venus}$ by 48 h.p.i. and continued to outperform $ZIKV_{venus}$ until 96 h.p.i., reaching final titers of 4.27×10^6 PFU/ml and 2.40×10^6 PFU/ml respectively compared to $ZIKV_{venus}$ that reached 6.93×10^5 PFU/ml, indicating that M_{F37L} and similar hydrophobic residues provide optimal growth advantage for ZIKV production in the absence of any C protein mutation.

The critical functions of C α3 and M-H1 are conserved in DENV

We next evaluated whether residues analogous to C α3 and M_{F37} of ZIKV are necessary for assembly in DENV, a closely related mosquito-borne flavivirus. Based on the NMR structure of DENV C protein (PDB:1R6R) [42], we selected surface-exposed residues L66, K67, and T71, as well as internally facing residues T62 and I65 on the C α3 for alanine substitution and further characterization of the mutants using DENV-2 16681 infectious cDNA clone pD2/IC-30P represented as $DENV_{WT}$ (Fig 8A) [52]. Viruses were generated by *in vitro* transcription and electroporation, and phenotypes were evaluated by plaque assays of the supernatant using BHK-15 cells (Fig 8B–8D). $DENV_{WT}$ formed plaques with an average diameter of 2.5±0.98 mm (Fig 8B and 8C) and resulted in a titer of 1.25×10^6 PFU/ml (Fig 8D). Compared to $DENV_{WT}$, the mutant viruses DENV-C_{L66A} and DENV-C_{K67A} produced significantly smaller plaques with an average diameter of 0.9±-.42 and 1.0±0.21 mm, and reduced titers, 1.87×10^3 and 1.23×10^4 PFU/ml respectively. DENV-C_{T71A} produced large plaque sizes with an average diameter of 2.0±0.59 mm, giving a 1.01×10^4 PFU/ml titer. Internally facing residue mutants DENV-C_{T62A} and DENV-C_{I65A} were non-plaque forming, likely due to compromised tertiary interactions at the C protein dimer interface. Additionally, we generated double mutants combining alanine substitutions of externally oriented residues [$_{66}LK_{67}/_{66}AA_{67}$ (DENV-Dm-1)] or [$_{67}KRWGT_{71}/_{67}ARWGA_{71}$ (DENV-Dm-2)], neither of which formed observable plaques. A multiple alanine substitution mutation [$_{62}TAGILKRWGT_{71}/_{62}AAGAAARWGA_{71}$ (DENV-Cm)] targeting the non-conserved and surface-exposed residues was also lethal. Finally, to determine whether the overall sequence specificity of α3 is significant, we generated a full α3 helix swap with DENV expressing the α3 sequence of ZIKV [(DENV-$_{62}$TA-GILKRWGT$_{71}$/$_{62}$SLGLINRWGSVI$_{71}$) (DENV-Sw)] which was also non-plaque forming.

The residue analogous to ZIKV M_{F37} is leucine in DENV (Fig 7B). To determine the importance of this residue in DENV, we first generated a DENV-M_{L37A} mutant which was attenuated, produced small plaques (1.2±0.50 mm diameter), and formed an average titer of 4.80×10^2 PFU/ml compared to $DENV_{WT}$ (2.5±0.98 mm diameter plaques) with a titer of 1.25×10^6 PFU/ml (Fig 8B–8D). When we substituted M_{L37} with the analogous residue from ZIKV to generate DENV-M_{L37F}, the mutant virus was less attenuated, with 1.6±0.38 mm diameter plaques and a titer of $9.87\text{x}10^4$ PFU/ml (Fig 8B–8D). We then compared the growth kinetics of DENV-C_{K67A}, DENV-C_{T71A}, and DENV-M_{L37F} with $DENV_{WT}$ in BHK-15 cells. Mutants with titers $<1.0\times10^4$ PFU/ml were not included in this assay. The growth rate of the DENV mutants was consistently lower than $DENV_{WT}$ (Fig 8E). The final average titers after 96 h.p.i. of DENV-C_{K67A}, DENV-C_{T71A}, and DENV-M_{L37F} were 1.92×10^5, 6.93×10^5, and 4.53×10^5 PFU/ml, respectively, compared to $DENV_{WT}$ which reached an average titer of 3.73×10^6 PFU/ml.

Discussion

The flavivirus C protein mediates viral RNA genome packaging and nucleocapsid budding into the ER lumen to form immature viral particles. We have identified a novel role for the α3

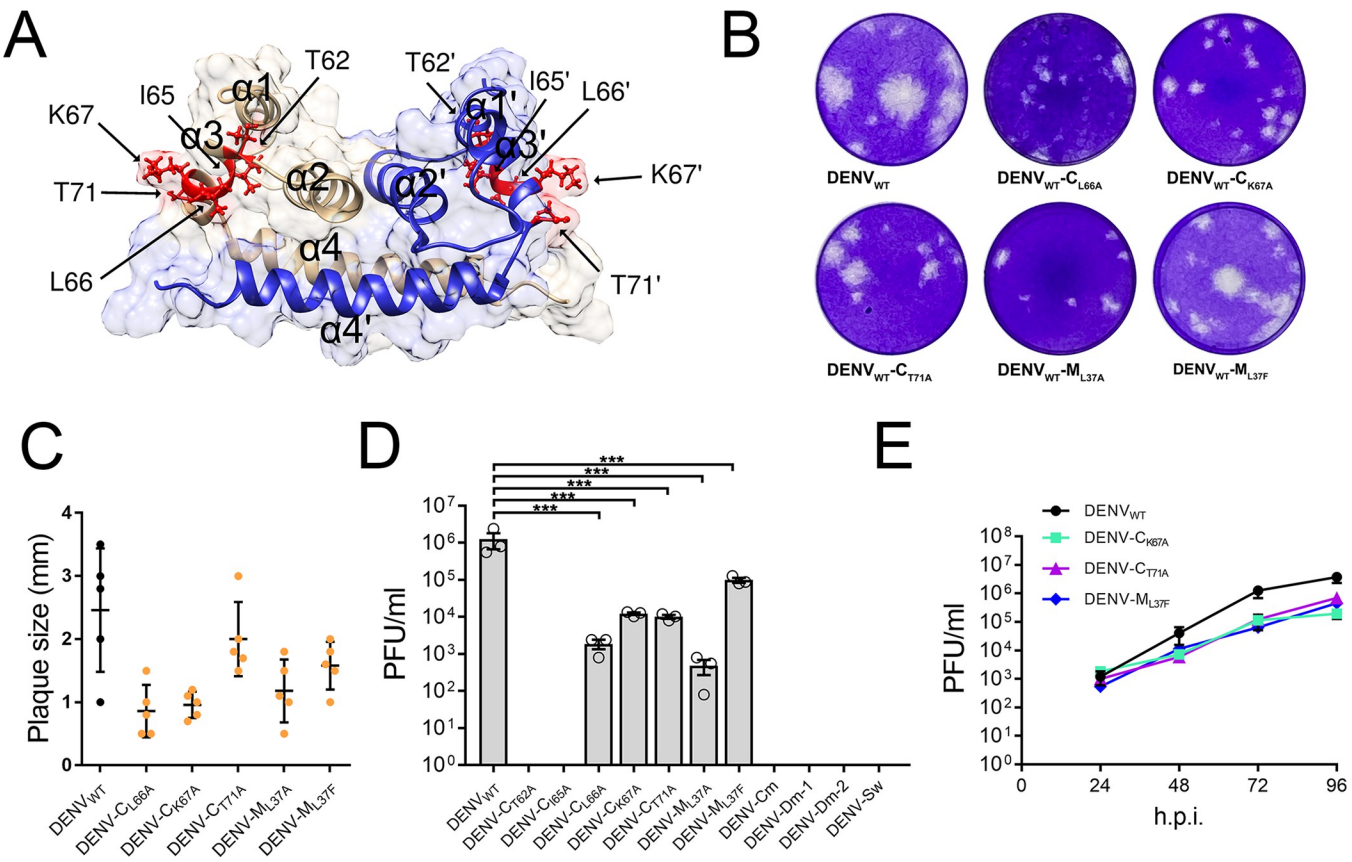

Fig 8. Mutational analysis of DENV C α3 and M_{L37}. (A) NMR structure of DENV C (PDB:1R6R) generated using UCSF Chimera software with α3 residues selected for mutational analysis shown as ball and stick and colored in red. Chain A is shown in beige, chain B is shown in blue, and helices α1–4 are labeled on the structure. (B) Plaque morphologies of $DENV_{WT}$ and plaque-forming C mutants L66A(DENV-C_{L66A}), K67A(DENV-C_{K67A}), and T71A(DENV-C_{T71A}), as well as plaque-forming M mutants L37A(DENV-M_{L37A}), and L37F(DENV-M_{L37F}) in BHK-15 cells fixed at 7 d.p.i. and stained with crystal violet. (C) The graph shows plaque diameters measured from $DENV_{WT}$ (black circles) or mutant DENV (orange circles) plaque assays shown in (B). The graph represents average plaque diameters (n = 5) with error bars representing SD. Statistical significance was calculated by Ordinary one-way ANOVA using GraphPad PRISM 7 software at a 95% confidence interval. Relative significance indicated by asterisks ($p<0.01$ = **, $p<0.001$ = ***, values with $p>0.05$ considered not significant (ns)). (D) Virus titers (passage 0) calculated from plaque assay in BHK-15 cells of wild-type and mutant DENV. DENV-Cm represents a combination mutant (C_{-62}TAGILKRWGT$_{71}$/$_{62}$AAGAAARWGA$_{71}$), DENV-Dm-1 represents a double mutant one (C_{-66}LK$_{67}$/$_{66}$AA$_{67}$), DENV-Dm-2 represents a double mutant two (C_{-67}KRWGT$_{71}$/$_{67}$ARWGA$_{71}$), and DENV-Sw represents helix swap mutant with ZIKV C α3 in place of DENV C α3 (C_{-62}TAGILKRWGT$_{71}$/$_{62}$SLGLINRWGSVI$_{73}$). The graph represents average titers (n = 3) with error bars representing SEM. Statistical significance was calculated by Ordinary one-way ANOVA using GraphPad PRISM 7 software at a 95% confidence interval. Relative significance is indicated by asterisks ($p<0.001$ = ***). (E) Growth curve analysis of WT DENV, DENV-C_{K67A}, DENV-$C_{T71A,}$ and DENV-M_{F37L} viruses (passage 0) in BHK-15 cells infected at MOI = 0.01. The graph represents average titers (n = 3) at 24-, 48-, 72-, and 96 h.p.i. with error bars representing SEM.

https://doi.org/10.1371/journal.pntd.0011873.g008

helix of a, *Aedes*-transmitted flavivirus C protein in orchestrating virion assembly through molecular genetics and biochemical analyses. While several studies have explored the function of C protein residues, few have attributed key roles for amino acids in the relatively short α3 helix. Based on available crystal structures of mosquito-borne flavivirus C proteins, surface exposed on C α3 is a common feature despite the non-conserved sequence (S3 Fig). JEV α3 mutations C_{K63} and C_{L66} to alanine resulted in mild impairment of virus production but were not lethal [40]. However, in West Nile virus, large truncations removing the entire α2 and α3 in a two-component recombinant virus system were tolerated, indicating that the importance of this region varies by virus [53]. Notably, most of these studies used virus-like particles, replicons, or similar systems that indirectly measure viral functions. Here, by using full-length infectious cDNA clones of ZIKV and DENV for mutational analyses, we have identified

homologous functions for surface exposed α3 residues in mediating flavivirus assembly and uncovered a genetic interaction with M protein that can only be detected using full-length cDNA clones generating infectious virus.

In many plus-strand RNA viruses, capsid protein binding to an RNA molecule is the switch that triggers nucleocapsid core formation via lateral interactions with nearby capsid proteins [54–57]. In alphaviruses, the capsid nucleation forms core-like particles in the absence of other structural proteins, requiring only a short nonspecific oligomer for initiation [58]. SARS-CoV-2 has been proposed to utilize intracellular liquid-liquid phase separation mechanisms in conjunction with a packaging signal for assembly [59]. Although the RNA binding regions of C in flaviviruses have been identified, the nucleation process and lateral interactions between C dimers required for nucleocapsid formation are still undetermined. Lethal mutations such as $C_{K31A,R32A}$ and $C_{K85A/K86A}$ have been shown to prevent assembly by indirectly interfering with genome packaging; however, these mutations have not been associated with the incorporation of nucleocapsid core into the immature virus particle [40]. Thus far, our study is the first to identify a specific residue of C protein that inhibits assembly without affecting the RNA binding or destabilizing the protein structure, thereby affecting capsid protein dimerization. The position of the α3 helix in the flavivirus C protein structure suggests that this alpha helix is an ideal candidate for lateral interactions between adjacent C proteins. Inter-dimer interactions may be critical during assembly; however, α3 has been overlooked in mutagenesis studies, presumably due to the lack of sequence conservation in this region. We have shown that alanine substitution of a single surface exposed asparagine C_{N67} in the α3 helix of ZIKV abrogates virus assembly, causing a lethal phenotype (Fig 1). The polar side chain of C_{N67} has the potential to form hydrogen-bonding interactions with nearby amino acids. Additionally, asparagine is known to form isopeptide bonds with lysine residues in unstructured protein regions during the capsid formation in bacteriophages such as HK97 [60]. Therefore, it is feasible for the solvent-exposed residue C_{N67} to be involved in an interaction with nearby C protein molecules via one of the positively charged residues in the long N terminal unstructured region such as K2, K5, K6, K7, K18, or K31, stabilizing the internal nucleocapsid core observed in the cryo-EM structures of immature ZIKV. Indeed, in the dimeric form of flavivirus C proteins, the α3 from each monomer is oriented perpendicular to the proposed RNA binding regions: α1 at the top and α4 at the bottom of the dimer. Together, the structural orientation and biochemical properties of C_{N67} presumably contribute to the lateral interactions between C proteins without obstructing the RNA packaging function. Our *in vitro* assays (Fig 2) indicate that C_{N67A} mutation does not lead to defects associated with protein folding, oligomerization, or RNA genome packaging and, therefore is presumably involved in another critical function required for virus assembly in infected cells.

During flavivirus infection, the C protein is primarily localized to the ER membrane, where it is co-translationally translocated and later in the secretory pathway as a structural component of the budded virus. However, after the NS2B/NS3 protease cleavage, the C protein has also been shown to localize to lipid droplets and the nucleus, specifically to the nucleoli in the infected cells [12,14,39]. Although the functional roles of C protein at these distinct subcellular locations remain unclear, it has been proposed that the lipid droplet binding sequesters the cleaved C protein away from assembly sites to prevent premature RNA genome packaging, whereas the functional role of C protein localizing to the nucleolus is not clearly understood [39]. In DENV, the membrane association of C protein has been linked to residues in a hydrophobic cleft, which appears to partially expose α2 based on NMR structure [39]. However, in the ZIKV dimer, the hydrophobic cleft is obstructed by α1 and the N-terminal disordered region from each C protein monomer, indicating that a different area of C protein likely mediates the membrane binding. Here, we tested the effect of C_{N67A} mutation in C protein

membrane association and subcellular localization using live cell imaging. We show that the subcellular localization of $C_{N67A,}$ specifically the colocalization with lipid droplets (Fig 3A and 3B) and the nucleoli (Fig 3C and 3D), are identical to wild-type C protein, confirming that the C protein membrane association is not dependent on residue C_{N67}.

The most likely stages of the flavivirus life cycle to be impacted by the perturbation of C protein are genome packaging and virus assembly because both processes rely on direct C protein interactions. Newly assembled immature flavivirus particles that bud into the ER lumen traffic through the Golgi apparatus, where virus maturation mediated by the furin cleavage of prM protein occurs before the mature virus exits the infected cell. As such, assembly defects can be detected from the lack of colocalization of C protein with the Golgi marker Giantin [29]. Immunofluorescence showed that ZIKV containing the C_{N67A} mutation is not efficiently colocalizing with Golgi, while dsRNA formation is unaffected, implicating defects in virus assembly (Fig 4A–4F). Further testing of the C_{N67A} mutant by qRT-PCR (Fig 4H) and western blot analysis (Fig 4I) demonstrated a significant reduction in the release of viral RNA and C protein, respectively, suggesting that the defect caused must be before virus particle release. Based on these results, we conclude that C_{N67A} is an assembly-specific mutation and is the first to our knowledge that prevents assembly via a single C residue.

We next performed amino acid substitutions based on multiple sequence alignment of flavivirus C proteins (Fig 1C) to test the required biochemical properties of site C_{67} (Fig 5A and 5B). We hypothesized that the size and polarity of asparagine are essential factors in its function, which was confirmed by $ZIKV_{venus}$ mutants in which hydrophobic residue substitutions C_{N67A}, C_{N67G}, and C_{N67L} resulted in non-plaque forming virus, whereas charged or polar residues C_{N67R} and C_{N67K} were tolerated and sustained plaque formation. Interestingly, the residue akin to ZIKV C_{67} in DENV is lysine, indicating a common function on C α3 despite the lack of sequence conservation. The functional role of C_{N67} likely relies on an electrostatic interaction not supported by hydrophobic residues. It requires a certain level of electron density that is met by asparagine and lysine but only partially sustained by arginine. Additionally, crystal structures show stabilizing interactions of C α3 with the backbone carbonyl oxygen of nearby residues. For example, there is an interaction between N64 and S71 in ZIKV (PDB:5YGH) as well as an interaction between D66 and R62 in WNV (PDB: 1SFK) [43,44]. The possibility that these interactions are critical and that C_{67} can only tolerate polar or charged residues is also supported by our data. Overall, these data suggest that the identity of the residue at position C_{67} plays a significant role in ZIKV assembly.

Our data also show the assembly defects of $ZIKV_{venus}$-C_{N67A} are restored by a second site M_{F37L} mutation on the M structural protein, obtained via natural reversion or site-directed mutagenesis (Fig 6A–6D). Since the defects caused by C_{N67A} were assembly-specific, we tested whether the assembly is restored in the C_{N67A}+M_{F37L} double mutant, and western blot of purified virus from infected cell supernatants confirmed the release of virus particles comparable to the wild-type levels (Fig 6E). It must be noted that the structural positioning of C_{N67} and M_{F37} places them on opposite sides of the viral lipid bilayer, making direct contact between these two residues impossible. Thus, our data provide new evidence for a genetic interaction between C and M proteins directly related to virus assembly. Our data connect several recent studies that have implicated M protein involvement in virus assembly. Mutational analysis of conserved residues on the peri-membrane helix (M-H1) of M in DENV showed that alanine substitution of four residues at the C terminal end (M_{E33}, M_{W35}, M_{L37} M_{R38}) has a significant reduction in particle assembly [61]. Although the study did not reveal any connection to capsid protein, it implicates the direct analog M_{F37} of ZIKV identified in our revertant screen. Another study on JEV using virus-like particles that contained only prM and E pointed to M_{I36F} as an assembly mutation. However, the host-specific defect did not impair assembly in

C636 mosquito cells. Since there is no C in the virus-like particle system, this study did not consider the potential interaction of M and C, which can only be observed when all structural proteins are present in an infectious virus [62]. A comparison of the virulence of the ZIKV NIID123 strain from South Asia and PRVABC59 from the Americas has identified a similar F to L reversion at amino acid 53 on M [63]. M_{F53L} mutation increased the virulence of the NIID123 strain, whereas the reciprocal M_{L53F} mutation in PRVABC59 had a negative effect. The substitution of F and L residues is strikingly similar to the M_{F37L} reported in the current study (Fig 7), where the $ZIKV_{venus}$-M_{F37L} had a significantly increased titer, whereas the reciprocal M_{L37F} substitution in DENV reduced virus titer (Fig 8). Notably in the cryo-EM structure of immature ZIKV (PDB: 6LNU), M_{F37} appears near E protein residue 407, which is a highly conserved isoleucine in flaviviruses.

Supported by previous studies, our experiments provide evidence for the critical importance of M protein in flavivirus assembly. To our knowledge, this is the first evidence of a genetic interaction between C and M in flaviviruses that is required to form infectious viral particles. Recent structural studies on flaviviruses, including Binjari, Usutu, and Spondweni viruses, have shown that the orientation of the internal membrane loop ($M_{51\text{-}57}$, ZIKV numbering) changes between immature and mature structures [16,17,23]. Based on our data, we propose that the internal orientation of $M_{51\text{-}57}$ facilitates interaction with C protein that is allosterically regulated by M-H1 residues. Although the immature ZIKV structure has been resolved to a moderate 9 Å resolution [27,31], it is conceivable that the hydrophobic residue at position 37 in M-H1 could interact with other amino acids or the viral lipid bilayer in a specific way that promotes virus assembly (Fig 9C). Notably, recent immature virus structures are obtained by selecting immature particles that underwent incomplete maturation during normal egress from the cell; as such, they have been exposed to the low pH environment that typically triggers furin cleavage. In contrast, structures obtained from NH_4Cl-treated neutral pH environments have not been exposed to maturation and low pH conditions and are more representative of nascent immature particle structures in the ER lumen [28]. In these immature virus structures, a density corresponding to the C protein is observed below the membrane, making direct contact with the internal portions of M and E proteins. Based on our results, we propose that M and C proteins coordinate the assembly of the immature particle, and that the interaction is lost due to the maturation-mediated glycoprotein rearrangement in the secretory pathway; therefore, the interaction is not observed in high-resolution cryo-EM structures of mature virions.

Finally, we validated the functional role of the C α3 helix in regulating virus assembly across *Aedes*-transmitted flaviviruses by performing a mutational analysis of DENV. Multiple alanine substitutions of five surface exposed side chains of α3 helix $_{62}$TAGILKRWGT$_{71}$/$_{62}$AA-GAAARWGA$_{71}$ (DENV-Cm), were lethal (Fig 8A and 8D), confirming the significance of the α3 helix. The alanine substitution of C_{T62} and C_{I65} residues with internally facing side chains was lethal because the interactions are likely crucial for C protein folding and dimerization (Fig 8A–8D). Unlike ZIKV, the mutation of a single surface exposed residue did not completely abrogate virus assembly in DENV. The two amino acid mutations, C_{L66A} and $C_{K67A,}$ resulted in 3-log and 2-log reductions in virus titer, respectively, with smaller plaque phenotypes, indicating the importance of these residues (Fig 8B and 8D). However, a double mutant combining two surface exposed residues, L66A+K67A (DENV-Dm-1) or L67A+T71A (DENV-Dm-2), resulted in a lethal phenotype (Fig 8D). Thus, we show that the functional role served by ZIKV C_{N67} is presumably orchestrated by a combination of residues L66, K67, and possibly T71 in the DENV C protein. We also created a complete helix substitution of DENV α3 helix with the α3 helix from ZIKV $_{62}$TAGILKRWGT$_{71}$/$_{62}$SLGLINRWGSVI$_{71}$ (Fig 8D, DENV-Sw), which was non-plaque forming, demonstrating the virus-specific amino acid

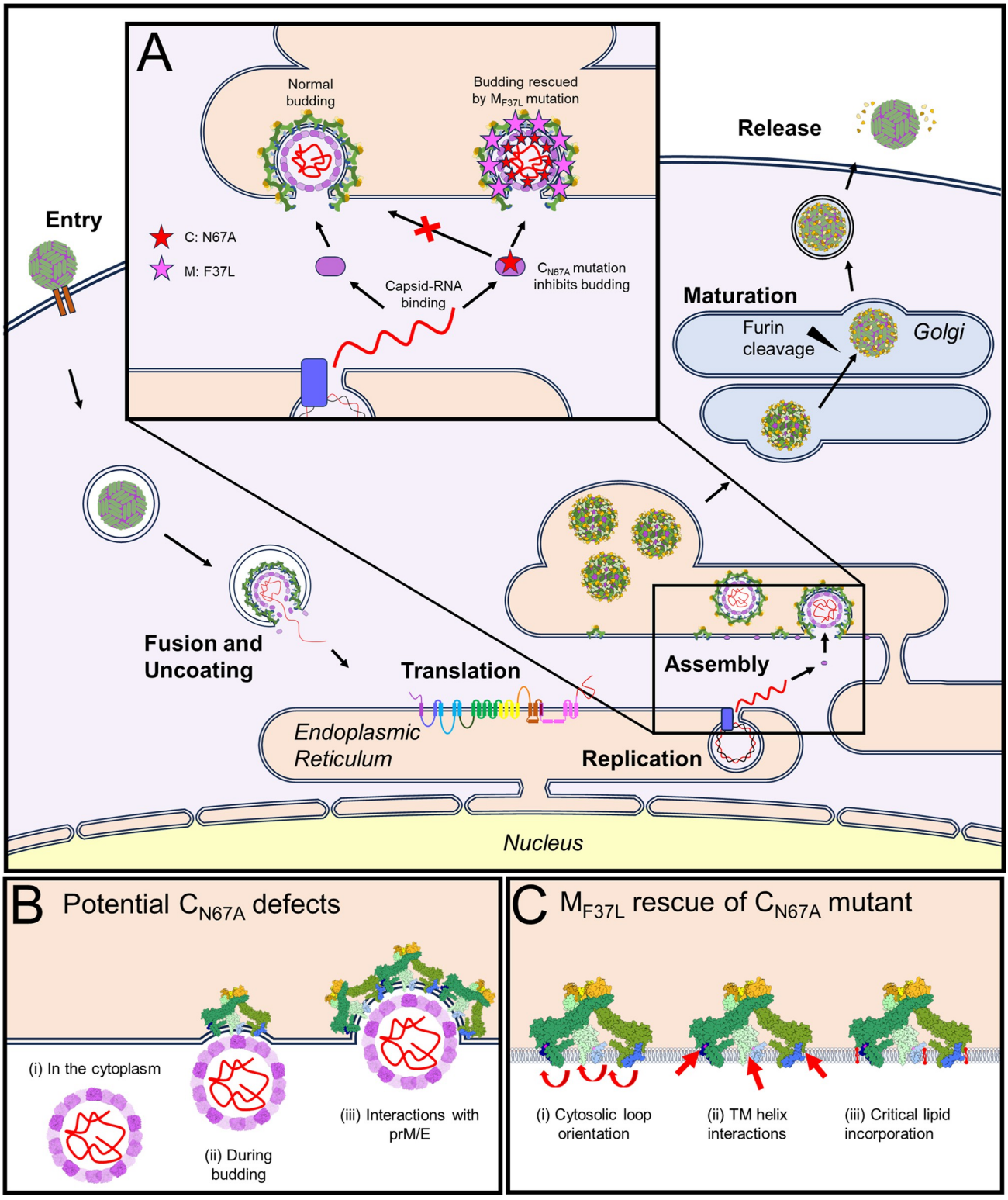

Fig 9. Proposed impacts of C_{N67A} and C_{N67A}+M_{F37L} mutations on flavivirus assembly. (A) In the wild-type virus, capsid protein (purple) and prM/E heterodimers (green and yellow) assemble along with viral RNA (red) and the lipid bilayer to generate immature viral particles (left). Mutation C_{N67A} (red star) prevents virus assembly, leading to a lack of immature particle budding. In C_{N67A}-M_{F37L} revertant (magenta star), assembly is restored (right). (B) Potential core formation defects caused by C_{N67A} mutation. (C) Potential mechanisms of M_{F37L} rescue of C_{N67A} mutant. Icons for flavivirus images were generated manually using PowerPoint and InkScape drawing tools with published cryo-EM structures of mature (PDB: 6CO8) and immature

(PDB:5U4W) ZIKV structures generated using ChimeraX as templates. All icons in A are drawn using Microsoft PowerPoint. Icons representing protein structures in B and C were generated using ChimeraX https://www.rbvi.ucsf.edu/chimerax.

https://doi.org/10.1371/journal.pntd.0011873.g009

sequence possibly required for the interactions in the function of C α3 because α3 is not a highly conserved region.

Based on the evidence presented in this study, we propose a model of *Aedes*-transmitted flavivirus assembly (Fig 9). Mutation of C_{N67} to alanine prevents assembly, indicating a critical function of the α3 helix (Fig 9A). In contrast, the second site M_{F37L} mutation rescues the assembly function, and immature viral particles can form (Fig 9A). The retention of dimerization and RNA binding activity indicates that the critical step affected by residue N67 is related to nucleocapsid core formation (Fig 9B). It is not currently known if core formation occurs prior to (i), in parallel with (ii), or during budding (iii), making it difficult to discern the defect caused by the C_{N67A} mutation. As for the M_{F37} residue, numerous possible mechanisms could be rescuing assembly, including (i) realigning the orientation of the M and E cytosolic loops to facilitate an interaction with C, (ii) creating a stabilizing interaction between the transmembrane regions of the M and E proteins that compensates for a loss of stability due to C_{N67A}, or (iii) incorporation of a critical lipid moiety into the virion that aids in the assembly of immature particles (Fig 9C). Future work exploring structural differences between the C_{N67A}+M_{F37L} and WT ZIKV virions will pinpoint the mechanisms involved in these crucial interactions.

There are currently no effective and approved antivirals for flaviviruses. Flavivirus assembly is a promising area for potential antiviral drug development because of the availability of near-atomic cryo-EM structures and crystal structures for all three structural proteins, C, prM, and E, crucial to producing infectious viruses. Assembly inhibitors have been effective against many viruses, including lenacapavir against HIV and DGAT1 inhibitors against HCV [64,65]. Notably, a few flavivirus assembly inhibitors are in development, including the DENV-2-specific ST148, which induces tetramerization of C protein dimers, resulting in improper incorporation of C into virions [66,67]. It is, therefore, essential to explore the functional role of the C protein in nucleocapsid formation and virus budding to pursue the development of assembly inhibitors. The evidence for the novel genetic interaction of C with M that we have obtained in this study will be instrumental in developing structure-based assembly inhibition strategies to serve as anti-flaviviral treatments.

Materials and methods

Viruses and cells

The DNA-launched ZIKV MR766 cDNA clones under a CMV promoter ($ZIKV_{WT}$) and with a Venus-tagged NS2A protein ($ZIKV_{venus}$) were used to generate wild-type and mutant ZIKV [68]. Human embryonic kidney (HEK-293T) cells were used to transfect ZIKV cDNA clones to generate virus stocks. African green monkey kidney cells (Vero E6) and Human Choriocarcinoma Cells (JEG-3) were used for plaque assays and confocal microscopy experiments, respectively. Wild-type and mutant DENV clones were generated using a cDNA clone of DENV-2 16681 (pD2/IC-30P) ($DENV_{WT}$) under a T7 promoter [69]. *In vitro* transcribed RNA from wild-type and mutant DENV were electroporated into Baby hamster kidney cells (BHK-15). Vero E6 and HEK-293T cells were maintained in Dulbecco's Modified Eagle's Medium (DMEM) (Thermo Fisher Scientific, #12800–082), BHK-15 cells were maintained in Eagle's Minimal Essential Medium (MEM) (Thermo Fisher Scientific, #41500–018), and JEG-3 cells were maintained in DMEM: Nutrient Mixture F-12 (DMEM/F-12) (Thermo Fisher Scientific, #12500–062). All media were supplemented with 10% fetal bovine serum (FBS)

(Avantor Seradigm, #97068–085), non-essential amino acids (Thermo Fisher Scientific, #11140–050), and 1x Penicillin-Streptomycin (Corning Inc., #30-002-CI) antibiotic. All cells were incubated at 37˚C and in the presence of 5% CO_2.

Sequence analysis and site-directed mutagenesis

Clustal Omega was used to generate multiple sequence alignments of flavivirus C protein and M protein regions [70]. Subsequently, Jalview software (University of Dundee, Scotland) was used to analyze and annotate the alignments [71]. Surface exposed residues of C α3 from the ZIKV C crystal structure (PDB: 5YGH) were selected for substitution to alanine using site-directed mutagenesis using Phusion DNA polymerase (New England Biolabs, #MO5305) and primers shown in S1 Table (IDT DNA Inc.). The reactions were treated with DpnI (New England Biolabs, R0176) followed by transformation of NEB Stable (New England Biolabs) *E. coli* cells and selection in Lysogeny Broth (LB) agar plates containing 100 ug/ml Ampicillin. Plasmid DNA was purified from isolated colonies using the EconoSpin spin column miniprep kit (Epoch, #2160–250) and sequenced to confirm the mutations at the Huck Genomics Core facility at Pennsylvania State University.

Transfection, *in vitro* transcription of cDNA clones, and electroporation

Plasmid DNA representing wild-type and mutant ZIKV cDNA were transfected into 2.4×10^5 HEK-293T cells grown on 24-well culture plates using Transfection Grade Linear Polyethylenimine Hydrochloride (PEI-Max) (Polysciences, #49553-93-7). Media over the cells were replaced with OptiMEM (Thermo Fisher Scientific, #22600–050) 20 min before transfection. The cDNA clone (250ng) was incubated with PEI-Max in Opti-MEM for 20 min and then added to the cells. After 14–16 hours, transfection media were replaced with DMEM supplemented with 10% FBS and incubated at 37˚C. Cell culture supernatants were collected 96 hours post transfection (h.p.t.) and stored at -80˚C or used to infect Vero E6 cells for fluorescence focus assays and plaque assays. Wild-type and mutant cDNA clones of DENV were digested with *Xba*I and *in vitro* transcribed using T7 RNA polymerase (New England Biolabs, #MO251S) as described previously [72]. Approximately 10 μg of *in vitro* transcribed viral RNA was electroporated into 2.8×10^6 BHK-15 cells using the BioRad Gene Pulser Xcell system in 0.2 mm cuvettes (BioRad, #1652086). Electroporated cells were incubated at 37˚C and in the presence of 5% CO_2. Supernatants were collected after seven days and stored at -80˚C or used to infect BHK-15 cells for plaque assays.

Microscopy and image acquisition

Fluorescence micrographs ZIKV infected Vero E6 cells were acquired at 10x magnification using DsFi3 camera fitted with Nikon A1R microscope using green excitation:488 nm and emission:500–550 nm filters. All confocal images were acquired using a Nikon A1R confocal microscope with heated 60x oil immersion objective and 1.4 numerical aperture. Live imaging was conducted in a live imaging chamber (Tokai Hit, Fujinomiya, Shizuoka Prefecture, Japan) supplied with 5% CO_2 maintained at 37˚C. Laser and emission band-passes used were as follows: blue, excitation of 405 nm and emission of 425–475 nm; green, excitation of 488 nm and emission of 500–550 nm; red, excitation of 561 nm and emission of 570–620 nm; and far-red, excitation of 640 nm and emission of 660–740 nm. Nikon NIS Elements software was used for all image acquisition and analysis. Nonlinear lookup tables (LUTs) were used to adjust brightness and contrast for clarity.

Fluorescence analysis and plaque assay

For fluorescence focus analysis, serial 1:10 dilutions of wild-type or mutant $ZIKV_{venus}$ diluted in MEM were used to infect 4.0×10^4 Vero E6 cells grown on 96-well plates. The relative size of the fluorescent foci was recorded, and representative images were acquired at 5 days post-transfection. All experiments were performed in triplicate. Plaque assays for ZIKV and DENV were performed using Vero E6 and BHK-15 cells, respectively. Cell monolayers grown on 24-well plates were infected with serial dilutions of viruses prepared in a dilution media of MEM supplemented with 10 mM HEPES (N-2-hydroxyethylpiperazine-N'-2-ethanesulfonic acid; Sigma Aldrich, #HO887). Plates were incubated at room temperature on a rocker for 10 minutes, then transferred to a 37˚C incubator for 50 minutes. After incubation, cells were overlayed with DMEM (ZIKV) or MEM (DENV) containing 1.5% colloidal cellulose (Sigma-Aldrich, #435244) and 1% FBS, and incubated at 37˚C. After a 6-day (ZIKV) or 7-day (DENV) incubation period, cells were fixed with neutral buffered formalin (10% formaldehyde containing 0.004 g/ml NaH_2PO_4, 0.0065 g/ml Na_2HPO_4, pH 7.4) for one hour. Fixing solution and overlay were aspirated and cells were washed with Phosphate buffered Saline (PBS) pH 7.4. Subsequently, the cells were stained with 0.05% Crystal violet stain (Sigma-Aldrich, #V5265) in 20% ethanol for 20 minutes. After washing with water, virus plaques were counted, and titers were calculated. All experiments were performed in triplicate.

Bacterial expression and purification of ZIKV C proteins

Using ligation-independent cloning, open reading frames coding for wild-type or mutant ZIKV C proteins were introduced into bacterial expression plasmid (Addgene, #29708) to express the C protein as N-terminal Maltose binding protein (MBP) fusions (MBP-C). The clones were confirmed by Sanger sequencing, and the plasmids were subsequently transformed into *E. coli* BL-21 bacterial cells. Cultures of BL-21 cells transformed with the expression plasmid were grown in 2xYT broth containing 30 μg/ml kanamycin to OD_{600} of 1 at 32˚C, and protein expression was induced by adding 0.2 mM IPTG. The cultures were then shaken overnight at room temperature, and cells were pelleted by centrifugation at 15,000 ×g for 15 minutes in a JLA 16.250 rotor in a Beckman Coulter Avanti JE centrifuge. For protein purification, cell pellets were resuspended in 1x PBS and sonicated using a Branson Sonifier-250. The lysates were clarified by centrifugation at 15,000 ×g for 20 minutes using JA 14.50 rotor in the Beckman Coulter Avanti JE centrifuge. Supernatants containing MBP-C fusion proteins were incubated with amylose resin (New England Biolabs, #E8021S) for 60 min at 4˚C. Protein-bound resin was loaded on to a gravity column and washed with 20 column volumes of 1x PBS containing 1 M NaCl, followed by 20 column volumes of 1x PBS to remove impurities. The MBP-C fusion proteins were eluted in 2 ml fractions with PBS containing 25 mM D maltose (Fisher Scientific, #6363-53-7). Aliquots of elution fractions were mixed with SDS-loading dye, incubated at 95˚C for 5 minutes to denature the protein, and evaluated by sodium dodecyl sulfate–polyacrylamide gel electrophoresis (SDS-PAGE) using self-prepared 11.5% acrylamide-bisacrylamide (Fisher Scientific, #BP 1408–1) gels. Fractions containing a 54 kDa band corresponding to the MBP-C fusion protein were pooled, diluted with water to achieve a final salt concentration of 50 mM, and loaded onto a HiTrap-Heparin-HP affinity column (Cytiva 17-0407-01) connected to AKTA pure 25M fast protein liquid chromatography system operating with Unicorn 7.1 software (GE Healthcare). After washing the column with 3 column volumes of PBS with 60 mM NaCl, a 60 mM to 1 M NaCl salt gradient was applied. MBP-C fusion proteins were eluted at an ion concentration of approximately 800 mM NaCl (~75 mS/cm). The molecular weight of both MBP-C fusion proteins was around 54 kDa as determined by SDS-PAGE.

Electrophoretic mobility shift assay (EMSA)

Purified wild-type or mutant MBP-C protein was buffer exchanged with PBS using Millipore 30 kDa concentrator to a final protein concentration of 0.2 mg/ml. A gene fragment representing the 5'UTR and C of ZIKV cloned under the T7 promoter was used to generate RNA via *in vitro* transcription using T7 RNA polymerase (New England Biolabs, #MO2515), and the RNA was purified using an RNA clean and concentrator kit (Zymo Research, #R1015). Binding reactions were prepared in which purified RNA and protein were mixed at increasing molar ratios in a buffer containing 20 mM Tris pH 7.4, 50 mM NaCl, and 10 mM $MgCl_2$. The binding reactions were allowed to occur at room temperature for 20 min and then separated on a 6% Acrylamide gel prepared in TBE-glycerol buffer (89 mM Tris base, 89 mM boric acid, 2 mM EDTA, and 8% glycerol). The gel was stained in ethidium bromide for 10 min, then washed in deionized water, imaged using the BioRad ChemiDoc XRS+ Molecular imager, and analyzed with Image lab software. All buffers were prepared with Diethyl pyrocarbonate (DEPC, Sigma # D5758) treated water to prevent RNA degradation.

Glutaraldehyde crosslinking assay

Purified wild-type and mutant MBP-C proteins at a concentration of 0.16 mg/ml in PBS were mixed with increasing concentrations of glutaraldehyde (Sigma Aldrich) in 50 μL reaction volumes. The reaction mix was incubated at room temperature for 20 min, and reactions were stopped by adding Tris pH 8 to 50 mM final concentration. The samples were mixed with SDS loading dye, heated to 70˚C for 5 min, and separated on a 10% acrylamide gel. The gel was stained with Coomassie blue, and the image was acquired using the BioRad ChemiDoc XRS + Molecular imager.

Subcellular localization of ZIKV C protein

The sequence corresponding to the wild type, or mutant ZIKV C protein was cloned into a CMV promoter-driven pcDNA 3.1(+) mammalian expression vector with an N-terminal mCherry tagged fusion protein. Plasmid DNAs were transfected into JEG-3 cells grown on a 35 mm glass-bottomed dish (IBIDI, #81218–200). Cells were co-transfected with a plasmid coding for GFP-tagged nucleolin (Addgene, #28176) to determine the colocalization of C protein with the nucleoli. The transfected cells were stained with a lipid droplet stain monodansylpentane (MDH) (Abgent, #SM1000A) to analyze the colocalization of C protein to lipid droplets. The cells were incubated with the stain for 30 min at 37˚C, and the excess stain was removed by washing thrice with 1x PBS. Media were replaced with Opti-MEM, and confocal images were acquired.

Immunofluorescence (IF) analysis

JEG-3 cells were grown on 0.13–0.16 mm thick glass coverslips (Thermo Fisher Scientific, #12-545-80) on 24-well plates. When the cell confluency reached 50–80%, cells were transfected with wild-type or mutant ZIKV plasmid cDNA clones using lipofectamine 2000 (Invitrogen, #11668–019). At six hours post-transfection, media were replaced with DMEM/F-12 supplemented with 2% FBS and incubated for 48 h at 37˚C and 5% CO_2. Cells were washed with PBS and fixed with 3.7% paraformaldehyde in PBS for 15 min at room temperature. Next, the cells were washed thrice with PBS and subsequently permeabilized with 0.05% Triton X-100 (VWR, #0694) for 15 min at room temperature. Cells were washed thrice with PBS to remove the detergent and then blocked with PBS containing 10 mg/ml bovine serum albumin (BSA) (Sigma, #A7906) for 1 h at room temperature. Cells were then probed with either combination

of primary antibodies against ZIKV C protein (1:150 dilution of rabbit polyclonal ZIKV C, GeneTex, #GTX134186), and Golgi (1:100 dilution of mouse polyclonal anti-Giantin (Abcam, #ab37266), or ZIKV C and flavivirus dsRNA (1:200 dilution of mouse monoclonal anti-dsRNA, Thermo Fisher Scientific, #10010500) for overnight at 4˚C. Primary antibodies were removed, cells were washed thrice with PBS and probed with secondary antibodies Tetramethylrhodamine isothiocyanate (TRITC) goat anti-mouse (Thermo Fisher Scientific) diluted 1:200 in BSA and AlexaFluor-647 far-red goat anti-rabbit secondary antibody (Thermo Fisher Scientific, #A32728) diluted 1:100 in BSA. After 1 h incubation at room temperature, secondary antibodies were removed, and cell nuclei were stained with Hoechst stain (Invitrogen) diluted to 0.2 μg/ml in PBS for 15 min. Cells were then washed one final time in PBS before mounting on glass slides with 1.2 mm thickness (VWR, 48300–026) using FluorSave (Millipore, #345789), and confocal images were acquired.

Quantitative reverse transcription PCR (qRT-PCR)

Virus particles from culture supernatants were purified as described for western blot analysis. The virus pellets were resuspended in 200 μl of PBS, and RNA was isolated using the GenCatch viral RNA miniprep purification kit (Epoch Life Science, 18–60050). All qRT-PCR experiments were performed using purified viral RNA and primers aligning to ZIKV M protein and ZIKV E protein (S1 Table) on the ZIKV genome as previously described [73], using Power SYBR-Green RNA to C_T 1-step kit from Applied Biosciences (#4389986). The number of RNA molecules was estimated from C_T values calculated using a standard curve generated from known concentrations of *in vitro* transcribed ZIKV RNA molecules. All reactions were carried out in triplicate using the Applied Biosystems QuantStudio 3 PCR system.

Western blot analysis

Viruses from culture supernatants were purified via ultracentrifugation, and western blot analyses were performed to detect virus particles released from infected cells. Briefly, Vero E6 cells were grown on T75 flasks and infected with wild-type virus, mutant virus, or mock-infected for 60 min at 37˚C in the presence of 5% CO_2. Cells were washed twice with PBS, and media were replaced. Cell culture supernatants were collected 2 d.p.i. by centrifugation at 15,000 ×g for fifteen min. This supernatant was loaded on a 1 ml cushion of 25% Sucrose in Tris-NaCl-EDTA (TNE) buffer in 13.2 ml round bottom tubes (Beckman Coulter, #344059). The samples were spun at 100,000 ×g for two hours in SW 41 Ti rotor using a Beckman Coulter TLX-Optima ultracentrifuge to pellet viral particles. The virus pellet was resuspended in 150 μl of 1x SDS loading dye, heated to 90˚C for 5 min, and separated in a 12.5% acrylamide (Fisher Scientific, #BP1408) gel (self-prepared) for electrophoresis. Proteins were transferred from the gel to a PVDF membrane (Cytiva Amersham, #10600021) using a BioRad Trans-Blot Turbo transfer system. The membrane was washed thrice in 1x Tris-buffered saline with 0.1% Tween 20 (VWR, #0777) (TBST) and blocked overnight at 4˚C in LI-COR Intercept Blocking buffer (LICOR #927–60001). The blot was probed with primary antibody against ZIKV C (GeneTex, #GTX134186) at a 1:1000 dilution in blocking buffer and incubated overnight at 4˚C with rocking. Subsequently, the membrane was washed four times with TBST and probed with goat anti-rabbit secondary antibody conjugated with horse radish peroxidase (Sigma Aldrich, A0545) at a 1:1000 dilution in the blocking buffer. After 1 h incubation at RT with rocking, the blot was developed using Super Signal WestPico PLUS Chemiluminescent substrate (Thermo Fisher Scientific, #34577) and imaged using the BioRad ChemiDoc XRS+ Molecular imager and analyzed with Image lab software.

Revertant screening

Supernatants from HEK 293-T cells transfected with $ZIKV_{venus}$ containing the C_{N67A} mutation were collected (passage 0) and used to infect Vero E6 cells grown on 6-well plates and incubated for 6 days. The supernatant was then harvested to infect new Vero E6 cells (passage 1). This process was repeated until the >100 cell fluorescent clusters were observed (passage 5). At this point, cells were harvested, and total RNA was extracted using a Zymo Research Quick-RNA miniprep RNA purification kit. From extracted RNA, regions corresponding to the C and prM (nt 1–1030), E (nt 693–1816 and nt 1212–2511), NS2A (nt 3545–4399), and NS3 (nt 4377–5272 and nt 5242–6528) were reverse transcribed using OneTaq One step 2x master mix (New England Biolabs, #M04825) using primers as listed in S1 Table. Amplicons were solution purified (Epoch Life Science, #2360050) and sequenced at the Huck Genomic Core facility at Pennsylvania State University. Sequences were analyzed using Serial Cloner and FinchTV (Geospiza Inc.) to identify second site mutations.

Virus growth kinetics

For growth kinetic analyses of ZIKV, Vero E6 cells grown to 80% confluence on 6-well plates were infected with wild-type or mutant ZIKV at a multiplicity of infection (MOI) of 1.0 for one hour at 37˚C. Cells were washed with PBS, and media was replaced with DMEM supplemented with 10% FBS, and incubation was continued at 37˚C with 5% CO_2. After 24, 48, 72, and 96 hours, 200 μl cell culture supernatant samples were collected and replenished with 200 μl fresh growth medium. Viruses released into the media were quantified using plaque assays on Vero E6 cells as described above. For DENV growth kinetics analysis, BHK-15 cells at 95% confluence grown on 24-well plates were infected with wild-type or mutant DENV at an MOI of 0.01 for one hour at 37˚C. Cells were washed with PBS, and media were replaced with MEM supplemented with 10% FBS. After 24, 48, 72, and 96 hours, 50 μl supernatant samples were collected from the infected cells and replaced with fresh growth medium. Virus particles released into the media were quantified using plaque assays on BHK-15 cells as described elsewhere.

Supporting information

S1 Fig. Predicted structures of alanine substitutions. AlphaFold predictions of (A) wild type ZIKV C, (B) C_{I66A}, (C) C_{N67A}, (D) C_{R68A}, (E) C_{S71A}, colored by confidence level (color key top right). All figures are overlayed with the crystal structure of wild type ZIKV C (PDB: 5YGH) (pale green).
(TIF)

S2 Fig. Size Exclusion Chromatography. A_{280} elution profiles of (A) MBP-C_{N67A}, (B) MBP-C, and (C) MBP ran at 0.5 ml/min on a Superdex 200 GL column (Cytiva) equilibrated with PBS containing 0.5M NaCl.
(TIF)

S3 Fig. Comparison of flavivirus capsid structures. Overlayed structures of ZIKV C (PDB: 5YGH) (pale green) with (A) DENV C NMR structure (PDB: 1R6R), (B) WNV C crystal structure (PDB: 1SFK) (orange), and (C) JEV C crystal structure (PDB: 5OW2) (pink). Zoomed box in each image shows α3 residue orientations as compared to ZIKV C.
(TIF)

S1 Table. List of primers used for mutagenesis and cloning. Mutated codons are underlined.
(DOCX)

Acknowledgments

We thank Dr. Matthew Evans, Icahn School of Medicine at Mount Sinai, for the ZIKV cDNA clones.

Author Contributions

Conceptualization: Anastazia Jablunovsky, Anoop Narayanan, Joyce Jose.

Data curation: Anastazia Jablunovsky, Anoop Narayanan.

Formal analysis: Anastazia Jablunovsky, Anoop Narayanan.

Funding acquisition: Joyce Jose.

Investigation: Anastazia Jablunovsky, Anoop Narayanan, Joyce Jose.

Methodology: Anastazia Jablunovsky, Anoop Narayanan, Joyce Jose.

Project administration: Joyce Jose.

Resources: Joyce Jose.

Software: Joyce Jose.

Supervision: Joyce Jose.

Validation: Anastazia Jablunovsky, Anoop Narayanan.

Visualization: Anastazia Jablunovsky, Anoop Narayanan.

Writing – original draft: Anastazia Jablunovsky, Anoop Narayanan, Joyce Jose.

Writing – review & editing: Anastazia Jablunovsky, Anoop Narayanan, Joyce Jose.

References

1. Diamond MS. Evasion of innate and adaptive immunity by flaviviruses. Immunol Cell Biol. 2003 Jun; 81 (3):196–206. https://doi.org/10.1046/j.1440-1711.2003.01157.x PMID: 12752684
2. Pierson TC, Diamond MS. The continued threat of emerging flaviviruses. Nat Microbiol. 2020 Jun; 5 (6):796–812. https://doi.org/10.1038/s41564-020-0714-0 PMID: 32367055
3. Waller C, Tiemensma M, Currie BJ, Williams DT, Baird RW, Krause VL. Japanese Encephalitis in Australia—A Sentinel Case. N Engl J Med. 2022 Aug 18; 387(7):661–2. https://doi.org/10.1056/NEJMc2207004 PMID: 36070717
4. Coyne CB, Lazear HM. Zika virus—reigniting the TORCH. Nat Rev Microbiol. 2016 Nov; 14(11):707–15. https://doi.org/10.1038/nrmicro.2016.125 PMID: 27573577
5. Hennessey M, Fischer M, Staples JE. Zika Virus Spreads to New Areas—Region of the Americas, May 2015–January 2016. 2016; 65(3). https://doi.org/10.15585/mmwr.mm6503e1 PMID: 26820163
6. Dejnirattisai W, Supasa P, Wongwiwat W, Rouvinski A, Barba-Spaeth G, Duangchinda T, et al. Dengue virus sero-cross-reactivity drives antibody-dependent enhancement of infection with zika virus. Nat Immunol. 2016 Sep; 17(9):1102–8. https://doi.org/10.1038/ni.3515 PMID: 27339099
7. Barrett ADT. Current status of Zika vaccine development: Zika vaccines advance into clinical evaluation. npj Vaccines. 2018 Jun 11; 3(1):24. https://doi.org/10.1038/s41541-018-0061-9 PMID: 29900012
8. Chong HY, Leow CY, Abdul Majeed AB, Leow CH. Flavivirus infection—A review of immunopathogenesis, immunological response, and immunodiagnosis. Virus Research. 2019 Dec; 274:197770. https://doi.org/10.1016/j.virusres.2019.197770 PMID: 31626874
9. Barnard TR, Abram QH, Lin QF, Wang AB, Sagan SM. Molecular Determinants of Flavivirus Virion Assembly. Trends Biochem Sci. 2021 May; 46(5):378–90. https://doi.org/10.1016/j.tibs.2020.12.007 PMID: 33423940
10. Sevvana M, Long F, Miller AS, Klose T, Buda G, Sun L, et al. Refinement and Analysis of the Mature Zika Virus Cryo-EM Structure at 3.1 Å Resolution. Structure. 2018 Sep 4; 26(9):1169–1177.e3.

11. Neufeldt CJ, Cortese M, Acosta EG, Bartenschlager R. Rewiring cellular networks by members of the Flaviviridae family. Nat Rev Microbiol. 2018 Feb 12; 16(3):125–42. https://doi.org/10.1038/nrmicro.2017.170 PMID: 29430005

12. Welsch S, Miller S, Romero-Brey I, Merz A, Bleck CKE, Walther P, et al. Composition and three-dimensional architecture of the dengue virus replication and assembly sites. Cell Host Microbe. 2009 Apr 23; 5(4):365–75. https://doi.org/10.1016/j.chom.2009.03.007 PMID: 19380115

13. Junjhon J, Pennington JG, Edwards TJ, Perera R, Lanman J, Kuhn RJ. Ultrastructural characterization and three-dimensional architecture of replication sites in dengue virus-infected mosquito cells. J Virol. 2014 May; 88(9):4687–97. https://doi.org/10.1128/JVI.00118-14 PMID: 24522909

14. Cortese M, Goellner S, Acosta EG, Neufeldt CJ, Oleksiuk O, Lampe M, et al. Ultrastructural Characterization of Zika Virus Replication Factories. Cell Rep. 2017 Feb 28; 18(9):2113–23. https://doi.org/10.1016/j.celrep.2017.02.014 PMID: 28249158

15. Miorin L, Romero-Brey I, Maiuri P, Hoppe S, Krijnse-Locker J, Bartenschlager R, et al. Three-dimensional architecture of tick-borne encephalitis virus replication sites and trafficking of the replicated RNA. J Virol. 2013 Jun; 87(11):6469–81. https://doi.org/10.1128/JVI.03456-12 PMID: 23552408

16. Newton ND, Hardy JM, Modhiran N, Hugo LE, Amarilla AA, Bibby S, et al. The structure of an infectious immature flavivirus redefines viral architecture and maturation. Sci Adv. 2021 May; 7(20):eabe4507. https://doi.org/10.1126/sciadv.abe4507 PMID: 33990320

17. Renner M, Dejnirattisai W, Carrique L, Martin IS, Karia D, Ilca SL, et al. Flavivirus maturation leads to the formation of an occupied lipid pocket in the surface glycoproteins. Nat Commun. 2021 Feb 23; 12 (1):1238. https://doi.org/10.1038/s41467-021-21505-9 PMID: 33623019

18. Plevka P, Battisti AJ, Sheng J, Rossmann MG. Mechanism for maturation-related reorganization of flavivirus glycoproteins. J Struct Biol. 2014 Jan; 185(1):27–31. https://doi.org/10.1016/j.jsb.2013.11.001 PMID: 24252771

19. Mukherjee S, Sirohi D, Dowd KA, Chen Z, Diamond MS, Kuhn RJ, et al. Enhancing dengue virus maturation using a stable furin over-expressing cell line. Virology. 2016 Oct; 497:33–40. https://doi.org/10.1016/j.virol.2016.06.022 PMID: 27420797

20. Li L, Lok SM, Yu IM, Zhang Y, Kuhn RJ, Chen J, et al. The flavivirus precursor membrane-envelope protein complex: structure and maturation. Science. 2008 Mar 28; 319(5871):1830–4. https://doi.org/10.1126/science.1153263 PMID: 18369147

21. Yu IM, Zhang W, Holdaway HA, Li L, Kostyuchenko VA, Chipman PR, et al. Structure of the immature dengue virus at low pH primes proteolytic maturation. Science. 2008 Mar 28; 319(5871):1834–7. https://doi.org/10.1126/science.1153264 PMID: 18369148

22. Vaney MC, Dellarole M, Duquerroy S, Medits I, Tsouchnikas G, Rouvinski A, et al. Evolution and activation mechanism of the flavivirus class II membrane-fusion machinery. Nat Commun. 2022 Jun 28; 13 (1):3718. https://doi.org/10.1038/s41467-022-31111-y PMID: 35764616

23. Khare B, Klose T, Fang Q, Rossmann MG, Kuhn RJ. Structure of Usutu virus SAAR-1776 displays fusion loop asymmetry. Proc Natl Acad Sci U S A. 2021 Aug 24; 118(34):e2107408118. https://doi.org/10.1073/pnas.2107408118 PMID: 34417300

24. Hardy JM, Newton ND, Modhiran N, Scott CAP, Venugopal H, Vet LJ, et al. A unified route for flavivirus structures uncovers essential pocket factors conserved across pathogenic viruses. Nat Commun. 2021 Jun 1; 12(1):3266. https://doi.org/10.1038/s41467-021-22773-1 PMID: 34075032

25. Pulkkinen LIA, Barrass SV, Domanska A, Överby AK, Anastasina M, Butcher SJ. Molecular Organisation of Tick-Borne Encephalitis Virus. Viruses. 2022 Apr 11; 14(4):792. https://doi.org/10.3390/v14040792 PMID: 35458522

26. Prasad VM, Miller AS, Klose T, Sirohi D, Buda G, Jiang W, et al. Structure of the immature Zika virus at 9 Å resolution. Nat Struct Mol Biol. 2017 Feb; 24(2):184–6.

27. Tan TY, Fibriansah G, Kostyuchenko VA, Ng TS, Lim XX, Zhang S, et al. Capsid protein structure in Zika virus reveals the flavivirus assembly process. Nat Commun. 2020 Feb 14; 11(1):895. https://doi.org/10.1038/s41467-020-14647-9 PMID: 32060358

28. Therkelsen MD, Klose T, Vago F, Jiang W, Rossmann MG, Kuhn RJ. Flaviviruses have imperfect icosahedral symmetry. Proc Natl Acad Sci U S A. 2018 Nov 6; 115(45):11608–12. https://doi.org/10.1073/pnas.1809304115 PMID: 30348794

29. Majowicz SA, Narayanan A, Moustafa IM, Bator CM, Hafenstein SL, Jose J. Zika virus M protein latches and locks the E protein from transitioning to an immature state after prM cleavage. npj Viruses. 2023 Nov 6; 1(1):4.

30. Blazevic J, Rouha H, Bradt V, Heinz FX, Stiasny K. Membrane Anchors of the Structural Flavivirus Proteins and Their Role in Virus Assembly. J Virol. 2016 Jul 15; 90(14):6365–78. https://doi.org/10.1128/JVI.00447-16 PMID: 27147734

31. DiNunno NM, Goetschius DJ, Narayanan A, Majowicz SA, Moustafa I, Bator CM, et al. Identification of a pocket factor that is critical to Zika virus assembly. Nat Commun. 2020 Oct 2; 11(1):4953. https://doi.org/10.1038/s41467-020-18747-4 PMID: 33009400

32. Allison SL, Tao YJ, O'Riordain G, Mandl CW, Harrison SC, Heinz FX. Two distinct size classes of immature and mature subviral particles from tick-borne encephalitis virus. J Virol. 2003 Nov; 77(21):11357–66. https://doi.org/10.1128/jvi.77.21.11357-11366.2003 PMID: 14557621

33. Garg H, Mehmetoglu-Gurbuz T, Joshi A. Virus Like Particles (VLP) as multivalent vaccine candidate against Chikungunya, Japanese Encephalitis, Yellow Fever and Zika Virus. Sci Rep. 2020 Mar 4; 10 (1):4017. https://doi.org/10.1038/s41598-020-61103-1 PMID: 32132648

34. Garg H, Sedano M, Plata G, Punke EB, Joshi A. Development of Virus-Like-Particle Vaccine and Reporter Assay for Zika Virus. J Virol. 2017 Oct 15; 91(20):e00834–17. https://doi.org/10.1128/JVI.00834-17 PMID: 28794019

35. Sotcheff S, Routh A. Understanding Flavivirus Capsid Protein Functions: The Tip of the Iceberg. Pathogens. 2020 Jan 5; 9(1):42. https://doi.org/10.3390/pathogens9010042 PMID: 31948047

36. Xie X, Zou J, Zhang X, Zhou Y, Routh AL, Kang C, et al. Dengue NS2A Protein Orchestrates Virus Assembly. Cell Host Microbe. 2019 Nov 13; 26(5):606–622.e8. https://doi.org/10.1016/j.chom.2019.09.015 PMID: 31631053

37. Zhang X, Xie X, Xia H, Zou J, Huang L, Popov VL, et al. Zika Virus NS2A-Mediated Virion Assembly. mBio. 2019 Oct 29; 10(5):e02375–19. https://doi.org/10.1128/mBio.02375-19 PMID: 31662457

38. Pong WL, Huang ZS, Teoh PG, Wang CC, Wu HN. RNA binding property and RNA chaperone activity of dengue virus core protein and other viral RNA-interacting proteins. FEBS Lett. 2011 Aug 19; 585 (16):2575–81. https://doi.org/10.1016/j.febslet.2011.06.038 PMID: 21771593

39. Samsa MM, Mondotte JA, Iglesias NG, Assunção-Miranda I, Barbosa-Lima G, Da Poian AT, et al. Dengue virus capsid protein usurps lipid droplets for viral particle formation. PLoS Pathog. 2009 Oct; 5(10): e1000632. https://doi.org/10.1371/journal.ppat.1000632 PMID: 19851456

40. Ishida K, Goto S, Ishimura M, Amanuma M, Hara Y, Suzuki R, et al. Functional Correlation between Subcellular Localizations of Japanese Encephalitis Virus Capsid Protein and Virus Production. J Virol. 2019 Oct 1; 93(19):e00612–19. https://doi.org/10.1128/JVI.00612-19 PMID: 31315991

41. Sangiambut S, Keelapang P, Aaskov J, Puttikhunt C, Kasinrerk W, Malasit P, et al. Multiple regions in dengue virus capsid protein contribute to nuclear localization during virus infection. J Gen Virol. 2008 May;89(Pt 5):1254–64. https://doi.org/10.1099/vir.0.83264-0 PMID: 18420804

42. Ma L, Jones CT, Groesch TD, Kuhn RJ, Post CB. Solution structure of dengue virus capsid protein reveals another fold. Proc Natl Acad Sci U S A. 2004 Mar 9; 101(10):3414–9. https://doi.org/10.1073/pnas.0305892101 PMID: 14993605

43. Shang Z, Song H, Shi Y, Qi J, Gao GF. Crystal Structure of the Capsid Protein from Zika Virus. J Mol Biol. 2018 Mar 30; 430(7):948–62. https://doi.org/10.1016/j.jmb.2018.02.006 PMID: 29454707

44. Dokland T, Walsh M, Mackenzie JM, Khromykh AA, Ee KH, Wang S. West Nile virus core protein; tetramer structure and ribbon formation. Structure. 2004 Jul; 12(7):1157–63. https://doi.org/10.1016/j.str.2004.04.024 PMID: 15242592

45. Morando MA, Barbosa GM, Cruz-Oliveira C, Da Poian AT, Almeida FCL. Dynamics of Zika Virus Capsid Protein in Solution: The Properties and Exposure of the Hydrophobic Cleft Are Controlled by the α-Helix 1 Sequence. Biochemistry. 2019 May 21; 58(20):2488–98.

46. Poonsiri T, Wright GSA, Solomon T, Antonyuk SV. Crystal Structure of the Japanese Encephalitis Virus Capsid Protein. Viruses. 2019 Jul 6; 11(7):623. https://doi.org/10.3390/v11070623 PMID: 31284608

47. Li T, Zhao Q, Yang X, Chen C, Yang K, Wu C, et al. Structural insight into the Zika virus capsid encapsulating the viral genome. Cell Res. 2018 Apr; 28(4):497–9. https://doi.org/10.1038/s41422-018-0007-9 PMID: 29467384

48. Khromykh AA, Westaway EG. RNA binding properties of core protein of the flavivirus Kunjin. Archives of Virology. 1996 Mar; 141(3–4):685–99. https://doi.org/10.1007/BF01718326 PMID: 8645104

49. Teoh PG, Huang ZS, Pong WL, Chen PC, Wu HN. Maintenance of dimer conformation by the dengue virus core protein α4-α4' helix pair is critical for nucleocapsid formation and virus production. J Virol. 2014 Jul; 88(14):7998–8015.

50. Figueira-Mansur J, Aguilera EA, Stoque RM, Ventura GT, Mohana-Borges R. Mutations in the dimer interfaces of the dengue virus capsid protein affect structural stability and impair RNA-capsid interaction. Sci Rep. 2019 Feb 26; 9(1):2829. https://doi.org/10.1038/s41598-019-39185-3 PMID: 30808916

51. Jumper J, Evans R, Pritzel A, Green T, Figurnov M, Ronneberger O, et al. Highly accurate protein structure prediction with AlphaFold. Nature. 2021 Aug; 596(7873):583–9. https://doi.org/10.1038/s41586-021-03819-2 PMID: 34265844

52. Akey DL, Brown WC, Dutta S, Konwerski J, Jose J, Jurkiw TJ, et al. Flavivirus NS1 structures reveal surfaces for associations with membranes and the immune system. Science. 2014 Feb 21; 343 (6173):881–5. https://doi.org/10.1126/science.1247749 PMID: 24505133

53. Schlick P, Taucher C, Schittl B, Tran JL, Kofler RM, Schueler W, et al. Helices α2 and α3 of West Nile Virus Capsid Protein Are Dispensable for Assembly of Infectious Virions. J Virol. 2009 Jun; 83 (11):5581–91.

54. Mukhopadhyay S, Chipman PR, Hong EM, Kuhn RJ, Rossmann MG. In Vitro-Assembled Alphavirus Core-Like Particles Maintain a Structure Similar to That of Nucleocapsid Cores in Mature Virus. J Virol. 2002 Nov; 76(21):11128–32. https://doi.org/10.1128/jvi.76.21.11128-11132.2002 PMID: 12368355

55. Wang JCY, Chen C, Rayaprolu V, Mukhopadhyay S, Zlotnick A. Self-Assembly of an Alphavirus Core-like Particle Is Distinguished by Strong Intersubunit Association Energy and Structural Defects. ACS Nano. 2015 Sep 22; 9(9):8898–906. https://doi.org/10.1021/acsnano.5b02632 PMID: 26275088

56. Twarock R, Stockley PG. RNA-Mediated Virus Assembly: Mechanisms and Consequences for Viral Evolution and Therapy. Annu Rev Biophys. 2019 May 6; 48(1):495–514. https://doi.org/10.1146/annurev-biophys-052118-115611 PMID: 30951648

57. Dykeman EC, Stockley PG, Twarock R. Packaging Signals in Two Single-Stranded RNA Viruses Imply a Conserved Assembly Mechanism and Geometry of the Packaged Genome. Journal of Molecular Biology. 2013 Sep; 425(17):3235–49. https://doi.org/10.1016/j.jmb.2013.06.005 PMID: 23763992

58. Snyder JE, Azizgolshani O, Wu B, He Y, Lee AC, Jose J, et al. Rescue of Infectious Particles from Pre-assembled Alphavirus Nucleocapsid Cores. J Virol. 2011 Jun 15; 85(12):5773–81. https://doi.org/10.1128/JVI.00039-11 PMID: 21471237

59. Chen H, Cui Y, Han X, Hu W, Sun M, Zhang Y, et al. Liquid–liquid phase separation by SARS-CoV-2 nucleocapsid protein and RNA. Cell Res. 2020 Dec; 30(12):1143–5. https://doi.org/10.1038/s41422-020-00408-2 PMID: 32901111

60. Tso D, Peebles CL, Maurer JB, Duda RL, Hendrix RW. On the catalytic mechanism of bacteriophage HK97 capsid crosslinking. Virology. 2017 Jun; 506:84–91. https://doi.org/10.1016/j.virol.2017.03.011 PMID: 28359902

61. Hsieh SC, Wu YC, Zou G, Nerurkar VR, Shi PY, Wang WK. Highly Conserved Residues in the Helical Domain of Dengue Virus Type 1 Precursor Membrane Protein Are Involved in Assembly, Precursor Membrane (prM) Protein Cleavage, and Entry. Journal of Biological Chemistry. 2014 Nov; 289 (48):33149–60. https://doi.org/10.1074/jbc.M114.610428 PMID: 25326389

62. De Wispelaere M, Khou C, Frenkiel MP, Desprès P, Pardigon N. A Single Amino Acid Substitution in the M Protein Attenuates Japanese Encephalitis Virus in Mammalian Hosts. Diamond MS, editor. J Virol. 2016 Mar; 90(5):2676–89.

63. Inagaki T, Taniguchi S, Kawai Y, Maeki T, Nakayama E, Tajima S, et al. Leu-to-Phe substitution at prM146 decreases the growth ability of Zika virus and partially reduces its pathogenicity in mice. Sci Rep. 2021 Oct 4; 11(1):19635. https://doi.org/10.1038/s41598-021-99086-2 PMID: 34608212

64. Bester S, Wei G, Zhao H, Adu-Ampratwum D, Iqbal N, Courouble VV, et al. Structural and mechanistic bases for a potent HIV-1 capsid inhibitor. Science. 2020 Oct 16; 370(6514):360–4. https://doi.org/10.1126/science.abb4808 PMID: 33060363

65. Herker E, Harris C, Hernandez C, Carpentier A, Kaehlcke K, Rosenberg AR, et al. Efficient Hepatitis C Virus Particle Formation Requires Diacylglycerol Acyltransferase 1 (DGAT1). Nat Med. 2010 Nov; 16 (11):1295–8.

66. Xia H, Xie X, Zou J, Noble CG, Russell WK, Holthauzen LMF, et al. A cocrystal structure of dengue capsid protein in complex of inhibitor. Proc Natl Acad Sci USA. 2020 Jul 28; 117(30):17992–8001. https://doi.org/10.1073/pnas.2003056117 PMID: 32669438

67. Scaturro P, Trist IML, Paul D, Kumar A, Acosta EG, Byrd CM, et al. Characterization of the Mode of Action of a Potent Dengue Virus Capsid Inhibitor. J Virol. 2014 Oct; 88(19):11540–55. https://doi.org/10.1128/JVI.01745-14 PMID: 25056895

68. Schwarz MC, Sourisseau M, Espino MM, Gray ES, Chambers MT, Tortorella D, et al. Rescue of the 1947 Zika Virus Prototype Strain with a Cytomegalovirus Promoter-Driven cDNA Clone. mSphere. 2016 Sep 28; 1(5):e00246–16. https://doi.org/10.1128/mSphere.00246-16 PMID: 27704051

69. Kinney RM, Butrapet S, Chang GJJ, Tsuchiya KR, Roehrig JT, Bhamarapravati N, et al. Construction of Infectious cDNA Clones for Dengue 2 Virus: Strain 16681 and Its Attenuated Vaccine Derivative, Strain PDK-53. Virology. 1997 Apr; 230(2):300–8. https://doi.org/10.1006/viro.1997.8500 PMID: 9143286

70. Madeira F, Pearce M, Tivey ARN, Basutkar P, Lee J, Edbali O, et al. Search and sequence analysis tools services from EMBL-EBI in 2022. Nucleic Acids Res. 2022 Apr 12; 50(W1):W276–9. https://doi.org/10.1093/nar/gkac240 PMID: 35412617

71. Waterhouse AM, Procter JB, Martin DMA, Clamp M, Barton GJ. Jalview Version 2—a multiple sequence alignment editor and analysis workbench. Bioinformatics. 2009 May 1; 25(9):1189–91. https://doi.org/10.1093/bioinformatics/btp033 PMID: 19151095

72. Leardkamolkarn V, Sirigulpanit W, Chotiwan N, Kumkate S, Huang CYH. Development of Dengue type-2 virus replicons expressing GFP reporter gene in study of viral RNA replication. Virus Res. 2012 Feb; 163(2):552–62. https://doi.org/10.1016/j.virusres.2011.12.007 PMID: 22197424

73. Tang WW, Young MP, Mamidi A, Regla-Nava JA, Kim K, Shresta S. A Mouse Model of Zika Virus Sexual Transmission and Vaginal Viral Replication. Cell Rep. 2016 Dec 20; 17(12):3091–8. https://doi.org/10.1016/j.celrep.2016.11.070 PMID: 28009279